Molecular Dynamics Study of Cholesterol Effects on Mechanical Rupture of Phospholipid Bilayer

TAIKI SHIGEMATSU

DECEMBER 2015

Molecular Dynamics Study of Cholesterol Effects on Mechanical Rupture of Phospholipid Bilayer

A dissertation submitted to

THE GRADUATE SCHOOL OF ENGINEERING SCIENCE

OSAKA UNIVERSITY

in partial fulfillment of the requirements for the degree of

DOCTOR OF PHILOSOPHY IN ENGINEERING

BY

TAIKI SHIGEMATSU

DECEMBER 2015

ABSTRACT

Cholesterol is one of the most essential molecule in phospholipid bilayers of animal cell membranes and is known to help to maintain the bilayer integrity under mechanical stresses without bilayer rupture. Although the bilayer rupture is critical for cell viability, the details of the cholesterol effects are still unclear. It is because the rupture process is divided into two stages, the formation of a nano-pore penetrating the bilayer and the spontaneous expansion of the pore, which are extremely fast processes and elusive in experiments. In order to understand the cholesterol effects on the bilayer rupture at the molecular level, a series of molecular dynamics simulations of stretched phospholipid bilayers containing cholesterol was performed. When the areal strain of the bilayer exceeded a critical value, water molecules permeated into the bilayer inside and a pore was formed. The critical areal strains for the cholesterol-containing bilayers were larger than that of the pure bilayer. The stretched cholesterol-containing bilayer formed an interdigitated gel phase like structure, in which the phospholipid and cholesterol molecules in one leaflet of the bilayer penetrated into the opposite leaflet and their orientations became ordered. The ordered bilayer structure after the phase transition might prevent the water permeation into the bilayer inside, which was an initiation of the pore formation, resulted in the higher critical areal strain of the cholesterol-containing bilayer. Moreover, the pore in the cholesterol-containing bilayer can spontaneously close even under higher areal strain than the pure bilayer. From the pore closure areal strain, the line tension of pore edge, which is an energetic loss per unit length, was estimated to increase with increasing the cholesterol concentration. This indicated that cholesterol facilitated the pore closure and prevented the pore expansion. In conclusion, behind the well-known cholesterol effects on the bilayer rupture, there were two molecular-level mechanisms. First, the stretch-induced phase transition to the interdigitated gel-like phase in the cholesterol-containing bilayer prevents the pore formation. Second, the higher line tension of the cholesterol-containing bilayer facilitates the pore closure and prevents the pore expansion. These findings will be fruitful to control the dynamics of pores and the subsequent membrane rupture in biological membranes, which are important problems in some medical treatments and experimental techniques for cell biology.

LIST OF ABBREVIATIONS

ANOVA	Analysis of Variance
LINCS	Linear Constraint Solver
MD	Molecular Dynamics
PME	Particle Mesh Ewald
QS	Quasistatic Stretching
RBC	Red Blood Cell
RDF	Radial Distribution Function
US	Unsteady Stretching

DPPC	1,2-dipalmitoyl-*sn*-glycero-3-phosphochline
1,3-DPPC	1,3-dipalmitoyl-*sn*-glycero-2-phosphochline
F-DPPC	1-palmitoyl-2-(16-fluoropalmitoyl)-*sn*-glycero-3-phosphocholine
DMPC	1,2-dimyristoyl-*sn*-glycero-3-phosphochline
DHPC	1,2-di-*O*-hexadecyl-*sn*-glycero-3-phosphocholine
SOPC	1-stearoyl-2-oleoyl- *sn*-glycero-3-phosphocholine
POPC	1-palmitoyl-2-oleoyl- *sn*-glycero-3-phosphocholine
DOPC	1,2-dioleoyl-*sn*-glycero-3-phosphochline
CHOL	Cholesterol

TABLE OF CONTENTS

CHAPTER 1.
INTRODUCTION

Cholesterol is an important component of biological cell membranes and occurs at a wide range of concentrations depending on the membrane type [1]. The roles of cholesterol in functions and physical properties of the membrane have long been recognized [2–4]. To understand the details of the cholesterol effects, the interactions between cholesterol and phospholipids, which are main components of the cell membranes and form a bilayer structure, have been comprehensively investigated. On the mechanical aspects, it is, for example, clarified that cholesterol reduces the passive permeability of water molecules across the bilayer [5], modulates the fluidity of the bilayer [6], induces the formation of micro-domains in the bilayer, called a lipid raft [7], and increases the mechanical stiffness of the bilayer [8]. Furthermore, at the molecular level, these cholesterol effects are considered to come from the ordering of phospholipids coexisting with cholesterols and subsequent condensation of the bilayer structure, which are called as ordering and condensing effects of cholesterol, respectively [9,10]. Progresses in understanding cholesterol effects in phospholipid bilayers at the molecular level have been summarized in excellent reviews over the years by several researchers [9,11–14].

Related to the cholesterol effects listed above, cholesterol in the bilayers is known to help to maintain the membrane integrity in situations where the membranes are exposed to various stresses. Needham and Nunn [8] performed a micropipette aspiration experiment for giant bilayer vesicles consisting of various phospholipids and cholesterol, and showed that the critical areal strain, where the rupture of the vesicle occurs, non-linearly changes with the cholesterol concentration. Koroniewicz and Kalinowski [15] performed an electroporation experiment using constant-current measurements for a planar bilayer containing cholesterol and showed that the presence of cholesterol in the bilayer causes an increase in the value of the breakdown potential. Both experiments suggest that cholesterol

increases the resistance of the bilayer to mechanical and electrical stresses, but the molecular details are not fully understood. Generally, animal phospholipid bilayers contain considerable amount of cholesterol molecule [1] and cholesterol effects on bilayer properties are profound. Thus, understanding the rupture of the cholesterol-containing bilayer is important for the development of various medical and experimental techniques that require delicate control of the permeability or failure of the biological membrane, e.g., electroporation [16], sonoporation [17], and ventricular assisted devices [18]. Furthermore, cholesterol is often employed as a stabilizer for synthetic bilayer vesicles, i.e., liposome, used for drug containers in drug delivery system [19,20]. Hence, to understand the molecular details of the cholesterol effects on the bilayer rupture can provide the fruitful knowledge for various medical and biological issues and is the aim of this study.

As the bilayer rupture is critical to cell viability, to clarify the details of the rupture mechanism, various experimental and theoretical studies have been performed. At the microscopic level, a pipette aspiration experiment for phospholipid bilayer vesicles is one of the commonest experimental technique and has yielded insights into the basic features of the bilayer rupture. Generally, the bilayer rupture occurs when the stress or strain of the bilayers exceed critical values, which depend, for example, on the lipid compositions of the bilayer (type of head group, unsaturation degree and length of tail groups, and, of course, cholesterol concentration) [21–23] and the time history of the applied stress or strain [23]. Evans and coworkers [23] reported experimental results about the latter: the rupture tension of pure phospholipid vesicles increases with increasing loading rate. They also interpreted their results based on a kinetic model for the bilayer rupture, in which the rupture process was modeled as a Markov process with a few intermediate states.

The basic idea used in the Evans's kinetic model was first proposed by Helfrich [24] and applied to the bilayer rupture by Litster [25]. The model has been long developed and used for explaining various membrane-related phenomena [26–29]. An important concept for the model of the bilayer rupture is dynamics of transmembrane pores in the phospholipid bilayer. The pore penetrates the

phospholipid bilayer and is filled with water molecules. At first, a pore is formed in the intact bilayer by external stresses. The pore is unstable and can close spontaneously. However, the pore can continue to expand indefinitely when once the pore exceeds a critical radius, leading to the bilayer rupture. From these, the rupture process can be divided into two processes: the pore formation in the intact bilayer and the subsequent pore expansion. As these processes are extremely fast, highly localized, and including complicated non-linear rearrangements of phospholipid and cholesterol molecules, the experimental observation or the theoretical prediction of the molecular details of the rupture process are difficult.

Molecular dynamics (MD) simulation of the bilayer is a promising method to reveal such molecular level phenomena in the bilayer [30]. In fact, MD simulation studies of various cholesterol effects in the unstressed bilayer [9,12,13] have been reported. Furthermore, several researchers, including our group, have performed MD simulations of the pore formation in the pure phospholipid bilayers under various stresses [31–34]. Nevertheless, MD simulations have not been applied to clarify the molecular details of the effect of cholesterol on pore formation and rupture under mechanical stresses.

In this study, in order to understand the molecular details of the cholesterol effects on the rupture of the bilayer under mechanical stresses, a series of MD simulation of stretched phospholipid bilayers containing cholesterol at various concentration is performed. As the rupture process can be considered to include two processes, pore formation and expansion, as described above, the simulations are also divided into two stages. In the first stage, MD simulations of stretched bilayers without a pore are performed to investigate the cholesterol effects on the pore formation stage in the rupture process. In the second stage, MD simulations of bilayers with a pre-formed pore are performed to investigate the cholesterol effects on the pore expansion stage in the rupture process. The details of the simulations for the two stages are described in the Chapter 2 and 3, respectively. Additionally, to develop understanding the cholesterol effects on the bilayer rupture, the interaction effects of cholesterol and

the stretching speed on the pore formation are investigated. The stretching speed is one of the important factor closely related to the bilayer rupture. For this objective, MD simulations of cholesterol-containing bilayers under stretching with various stretching speed are performed and details of the simulations are described in the Chapter 4. Finally, in the Chapter 5, conclusions of this study are stated.

CHAPTER 2.
CHOLESTEROL EFFECTS ON PORE FORMATION IN STRETCHED PHOSPHOLIPID BILAYER

2.1. INTRODUCTION

Cholesterol molecules in phospholipid bilayers are known to enhance the bilayer toughness to mechanical stresses and help to maintain the membrane integrity [8,22,35]. Despite there are many reports about the cholesterol effects, the molecular-level mechanism is not fully understood. From theoretical and experimental studies of the bilayers under mechanical and electrical stresses, the irreversible breakdown of the bilayer (rupture) is estimated to occur through two stages. In the first stage, unstable transmembrane pores are transiently formed in intact bilayers by external stresses. Accordingly, in the second stage, the pore expands spontaneously and indefinitely, resulting the bilayer rupture. The pore formation is a very fast and local event, involved in the molecular level structural changes of the bilayer. Thus, the role of cholesterol molecules in the pore formation in the rupture process is still unknown.

In this chapter, in order to understand the cholesterol effects on the pore formation, a series of molecular dynamics simulations of stretched dipalmitoylphosphatidylcholine (DPPC) bilayers containing different concentrations of cholesterol (0, 20, 40, and 60 mol%) is performed. From the trajectories of the stretched bilayers, how the processes of pore formation, the critical area where the pore is formed, and the molecular orientations in the stretched bilayers are related to the concentration of cholesterol are analyzed. Furthermore, the relationships between the resistance of the bilayer to pore formation and the change of the membrane structure induced by stretching are discussed. These analyses will reveal the difference of the molecular mechanism of the pore formation process in the phospholipid/cholesterol bilayers with different compositions of lipid and cholesterol molecules, and

provide insight into the toughness of red blood cell (RBC) membranes.

2.2. METHODS

2.2.1. Bilayer Systems

Planar phospholipid/cholesterol bilayer systems with cholesterol concentrations of 0, 20, 40, and 60 mol% were used. Each system comprised 200 lipid molecules of DPPC and cholesterol molecules in rectangular simulation boxes with periodic boundary conditions. To avoid the effects of the periodic images in the bilayer normal direction during stretching, a large number of water molecules (at least 11,918) were added to the systems. The pure DPPC bilayer and DPPC/cholesterol bilayers with 20, 40, and 60 mol% cholesterol were labeled as S00, S20, S40, and S60, respectively. DPPC and cholesterol molecules were represented by the united atom force fields for DPPC [36] and cholesterol [37], and water molecules by the simple point charge model [38]. For the equilibration, constant temperature (T) and pressure (P) MD simulations were performed for 100 ns at T = 323 K and P = 1 bar. The details of the system construction, simulation parameters for the equilibrium simulation, and structural properties of DPPC/cholesterol bilayers in equilibrium states are summarized in the Appendix A1. The structural properties of the four bilayers were in agreement with those obtained by experimental measurements [10,39–41] and previous simulations [42–44]. All MD calculations were performed with the GROMACS molecular dynamics simulation codes [45,46]. All snapshots were rendered using Visual Molecular Dynamics [47].

2.2.2. Stretching Simulations

The equilibrated bilayers prepared above were first stretched by the unsteady and equibiaxial stretching algorithm [32], and the stretched bilayers in desired areas were taken from the trajectories. Constant $NP_zA_{\parallel}T$ MD simulations of the bilayers [48] were performed for 100 ns at a constant temperature (T = 323 K), pressure in the z direction (P_z = 1 bar), and various areas ($A_{\parallel}$). $A_{\parallel}$ was set to

satisfy the areal strain ε_A = 0.2, 0.4, 0.6, 0.8, 1.0, 1.2, and 1.4, as explained below. To statistically analyze the critical areal strain where the pore forms, stretching simulations were performed starting from three different configurations taken from the trajectory of the equilibrated bilayers. The simulation parameters were essentially the same as those for the equilibrium simulations (see Appendix A1) except that the barostat method (Berendsen algorithm [49]) was used in the stretching simulations. It took about 3.6×10^3 CPU hours on a Linux cluster with 2.21 GHz Opteron processors for the S40 system under the areal strain ε_A = 1.0.

2.2.3. Analysis

The areal strain was defined by $\varepsilon_A = A_{\parallel}/A_0 - 1$, where $A_{\parallel}$ is the area of the simulation box upon stretching, and A_0 is the reference value obtained from the average for the last 50 ns of the equilibrated MD simulation. Pore formation in the bilayer was examined by visual inspection of the snapshots for each areal strain condition. It should be noted that because the areas were discretized in the stretching simulations, to more accurately estimate the critical strain ε_c, not only the minimum value of areal strain with a pore (ε_P) but also the maximum value without a pore (ε_I) during the stretching simulations were analyzed, and the actual critical strain can be found in the range from ε_I to ε_P.

Ordering in the hydrophobic tails of the lipid molecules was evaluated by the averaged order parameter:

$$\bar{S}_{CD} = \frac{1}{N_C}\sum_{i=1}^{N_C}\left(S_{CD}\right) = \frac{1}{N_C}\sum_{i=1}^{N_C}\left(-\frac{1}{4}\left\langle 3\cos^2\Theta_i - 1\right\rangle\right), \tag{2.1}$$

where Θ_i is the angle between the axis of the ith molecular axis and the bilayer normal (the z axis), N_c is the number of carbons in the lipid chains, and the brackets denote both ensemble and the time average. In this study, N_c was the number of carbons in the *sn*-2 chains (N_c = 14). Furthermore, to analyze the orientations of the cholesterol molecules in the stretched bilayers, the cholesterol tilt angle parameter was defined as

$$A_C = \left\langle \cos^2 \theta_C \right\rangle, \tag{2.2}$$

where θ_c is the instantaneous angle between the segmental vector, which is the vector between the carbon atoms of the ring structure connected to the tail (C21) and the hydroxyl group (C5) (see Fig. A1.1), and the bilayer normal (the *z* axis). If most of the cholesterol molecules are normal to the bilayer plane (the *x*-*y* plane), A_c will be close to 1, whereas if they are not, it will be close to 0. To analyze the association between the cholesterol molecules, the lateral radial distribution function (RDF) [42] between C21 carbon atoms in the cholesterol molecules for the bilayer plane (the *x*-*y* plane) was calculated in the individual layers and between layers.

2.3. RESULTS

2.3.1. Pore Formation Process

Figure 2.1 shows representative snapshots of the stretched DPPC/cholesterol bilayers for S40. With increasing the applied areal strain of the bilayer, the thickness monotonically decreases (Fig. 2.1, *A*–*F*) and, when the areal strain exceeds a critical value, water molecules penetrate into the hydrophobic region of the bilayer and bridge the bilayer (Fig. 2.1 *E*). The water bridge rapidly grows (Fig. 2.1 *F*), but is not clearly lined with the hydrophilic headgroups (i.e., it is similar to a hydrophobic pore) (Fig. 2.2 *right column*), unlike the case of the formation of hydrophilic pore for S00 (Fig. 2.2 *left column*) and for other stretched pure lipid bilayers [31,50]. This difference may be explained by the difference in line tensions between the hydrophilic and the hydrophobic pore in the bilayer [51]. In addition, there is a remarkable difference in the molecular orientations in the stretched bilayers. For the system S00 (i.e., a pure lipid bilayer), the DPPC molecules continue to tilt or spread their hydrophobic tails until pore formation (insets in Fig. 2.1, *G*–*I*). For the systems containing cholesterol, the DPPC and cholesterol molecules initially tilt, but then recover (see insets in Fig. 2.1 *C*).

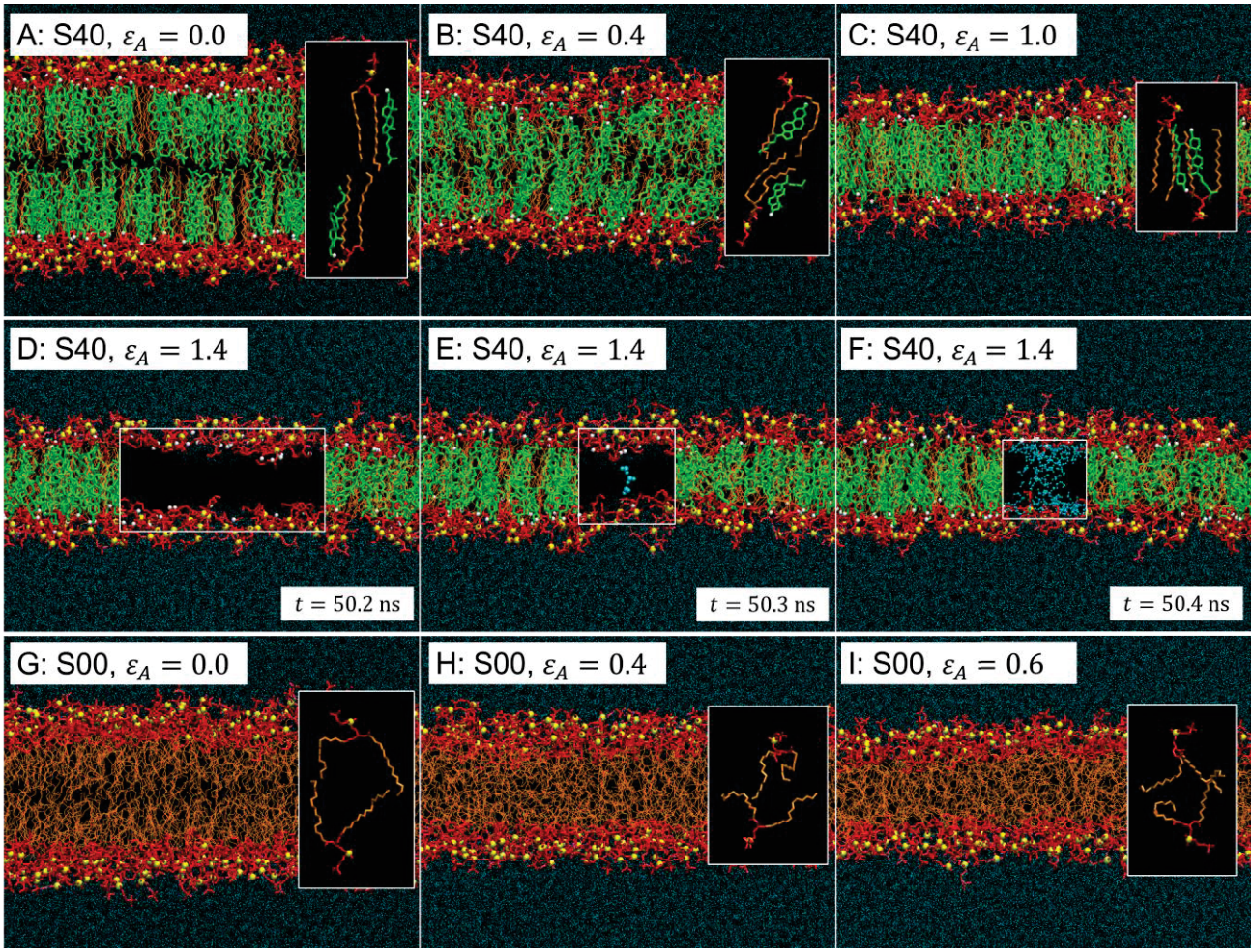

FIGURE 2.1 Representative snapshots of the stretched bilayers for S40 (*A*–*F*) and S00 (*G*–*I*). The applied areal strains are 0.0 (*A* and *G*), 0.4 (*B* and *H*), 0.6 (*I*), 1.0 (*C*), and 1.4 (*D*–*F*). The DPPC headgroups are shown in red, the DPPC tails in orange, the cholesterol molecules in green, phosphorus atoms of the DPPC as yellow spheres, hydrogen atoms of the cholesterol molecules as white spheres, and the water molecules in blue. In the sections shown in the white frames in panels *D*–*F*, the DPPC tails and cholesterol molecules are not shown, and the water molecules in the hydrophobic part of the membrane are emphasized for clarity. The insets in panels *A*–*C* and *G*–*I* are representative positions and orientations of the DPPC and cholesterol molecules.

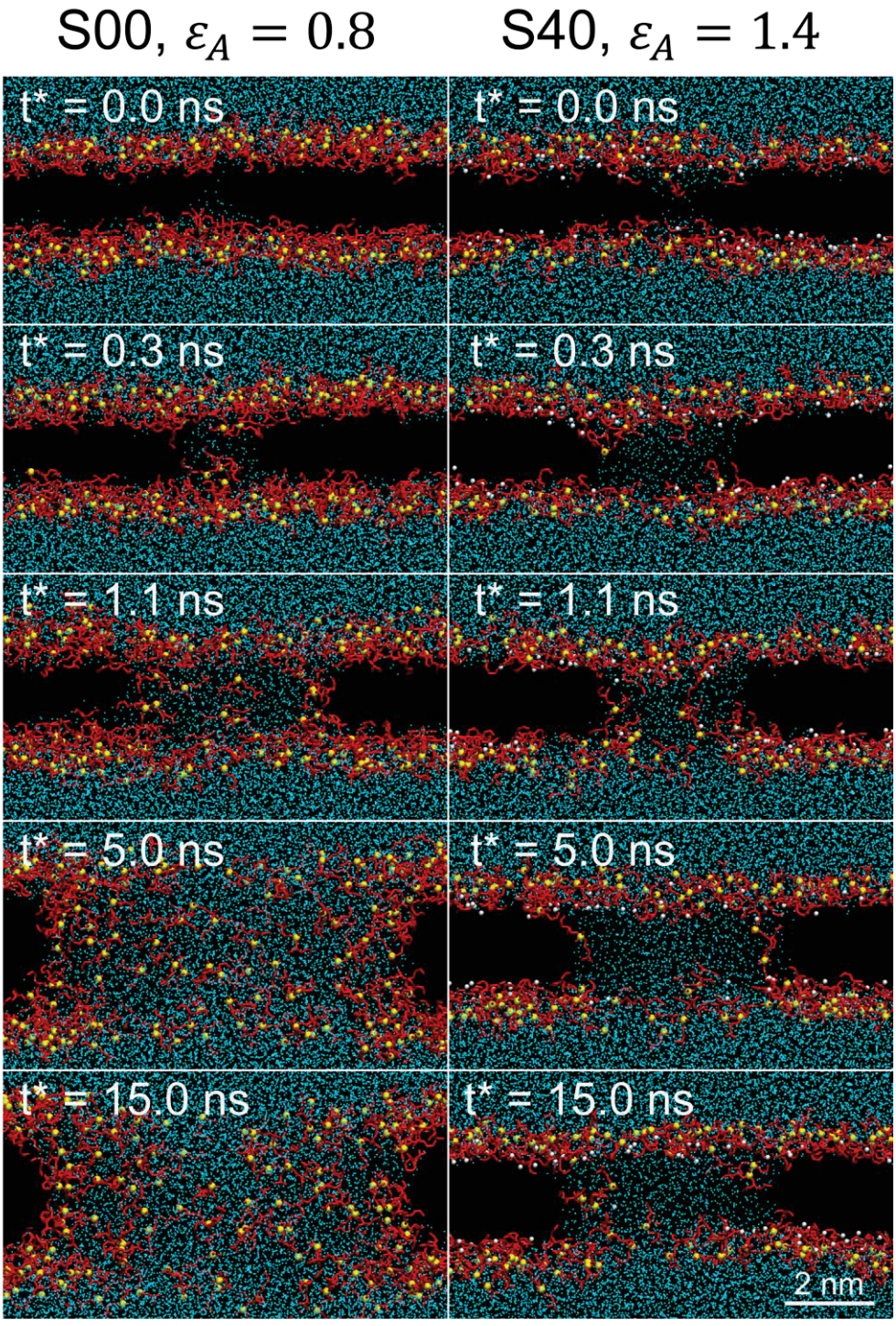

FIGURE 2.2 Representative snapshots of the pore growth processes for S00 (left column) and S40 (right column). The DPPC headgroups are shown in red, phosphorus atoms of the DPPC as yellow spheres, hydrogen atoms of the cholesterol molecules as white spheres, and the water molecules in blue. The DPPC tails and cholesterol molecules are not shown for clarity. t* in each panel shows the time that elapses after the formation of the water bridge.

2.3.2. Critical Areal Strain

The ε_P and ε_I values obtained for the four systems are shown in Fig. 2.3. Both ε_P and ε_I initially increase, peak at 40 mol%, and then decrease with increasing amount of cholesterol up to 60 mol%. As the areas were discretized in the stretching simulation, this indicates that the actual critical areal strain ε_c follows the same trend of ε_P and ε_I (gray region in Fig. 2.3). The results of the critical areal strains of the phospholipid/cholesterol bilayer agree well with previous experimental observation (peak at 30–40 mol%) [8]. It should be noted that the range of ε_c obtained here is about two orders of magnitude higher than that reported in the experiments, which can be explained by the small size of the system [29] (see also Appendix A1).

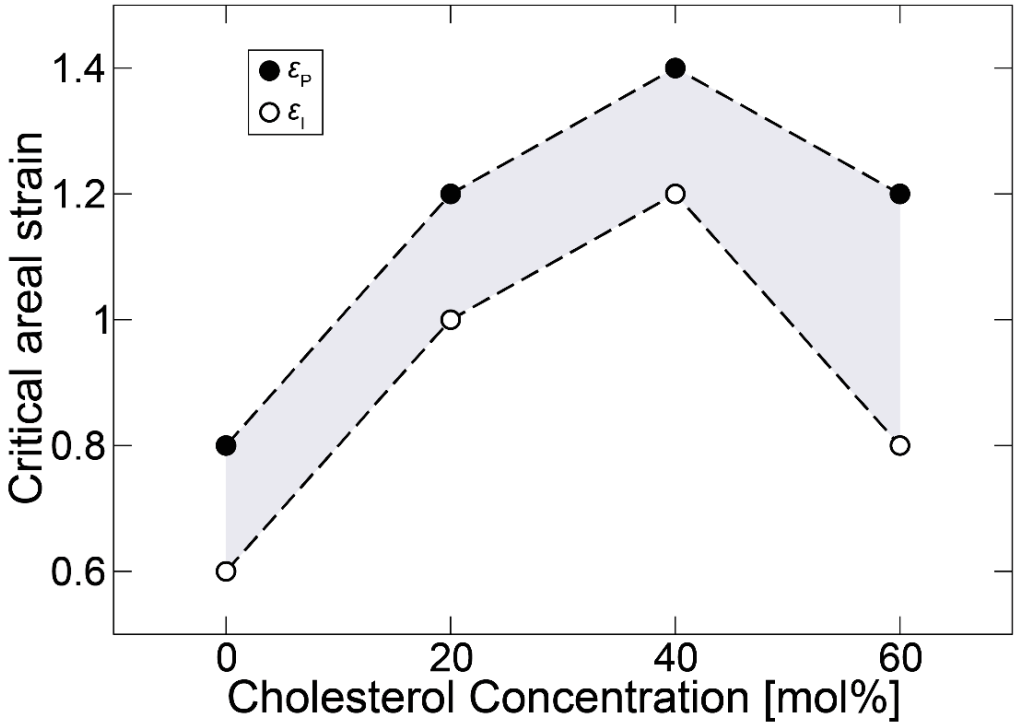

FIGURE 2.3 Minimum areal strain ε_P where the pore forms and maximum areal strain ε_I where the pore does not form as a function of the cholesterol concentration. The dashed lines show the linearly interpolated lines between the points, and the region, where the real critical areal strain is expected to be found, is shown in gray.

2.3.3. Molecular Orientation

In the phospholipid/cholesterol bilayer, the orientations of the DPPC and cholesterol molecules depended on the applied areal strain (Fig. 2.1). The relationships between the averaged order parameter $\overline{S}_{CD}$ and the areal strains, and between the cholesterol tilt angle parameter A_c and the areal strains for the four systems, are shown in Fig. 2.4, *A* and *B*, respectively. Both parameters initially decrease and then begin to increase when the applied areal strain exceeds 0.4 or 0.6. From the distributions of $\overline{S}_{CD}$ in the *sn*-2 hydrophobic tail for S40 (Fig. 2.5), it is clear that the recovery of $\overline{S}_{CD}$ is because of the recovery of the order at the distal end of the hydrophobic tails.

The recovery of $\overline{S}_{CD}$ and A_c is prominent for S40. The association of cholesterol molecules was analyzed by using the lateral RDFs between the C21 carbon atoms of the cholesterol molecules (Fig. 2.6, *A* and *B*). Based on the transitional change of $\overline{S}_{CD}$ for the system S40 in Fig. 2.4 *A*, the stretching process can be divided into two stages: the low areal strain stage (ε_A = 0.0–0.4) and the high areal strain stage (ε_A > 0.4). In the low areal strain stage, the peak heights of the RDFs decrease with increasing areal strain, except for the peak at about 0.7 nm (Fig. 2.6 *A*). On the other hand, in the high areal strain stage, the peaks become higher with increasing areal strain up to 1.0 (Fig. 2.6 *B*).

The RDFs between the C21 carbon atoms in the upper and lower layers are useful to understand the interactions of cholesterol molecules between the layers (Fig. 2.6 *C*). In the low areal strain stage, the RDFs do not have peaks, indicating that there is no significant interaction of cholesterol molecules between the layers. On the other hand, in the high areal strain stage, some peaks appear at small radial distances, indicating that the interaction between cholesterol molecules of the upper and lower layers becomes significant. In particular, the profile of the RDF between cholesterol molecules of the upper and lower layers for ε_A = 1.0 (thick dashed line in Fig. 2.6 *C*) is similar to that for ε_A = 0.0 (see Fig. A1.2). Figure 2.7 shows representative snapshots of the cholesterol molecule orientations and distributions for ε_A = 0.0 and 1.0. The two monolayers in the bilayer interpenetrate for ε_A = 1.0 (Fig. 2.7 *bottom-right*), forming an interdigitated gel-phase-like structure [52]. In the interdigitated bilayer,

cholesterol molecules are localized and form domains (Fig. 2.7 *top-right*), whereas the localization of DPPC molecules is indistinct.

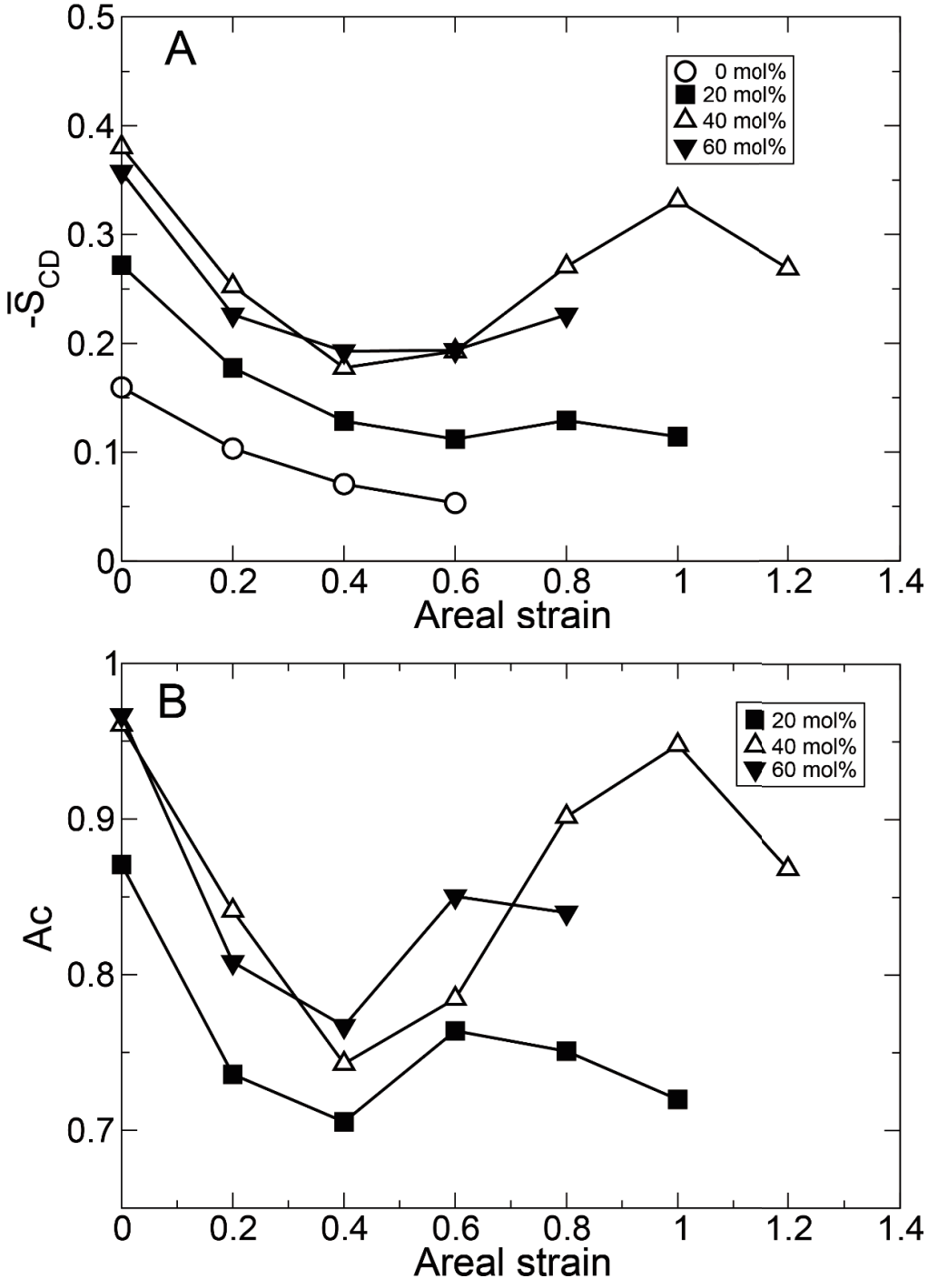

FIGURE 2.4 (*A*) Average lipid chain order parameter $\overline{S}_{CD}$ and (*B*) cholesterol tilt angle parameter A_C versus areal strain.

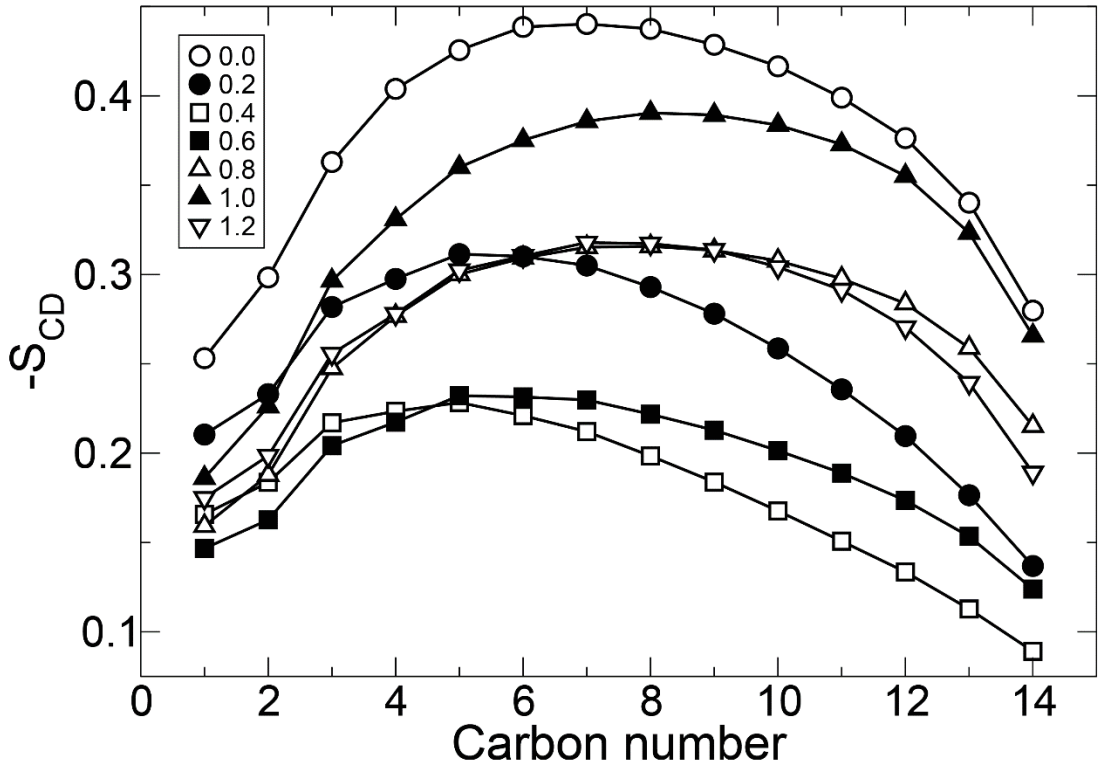

FIGURE 2.5 Variation of lipid order parameter for S40 with $\varepsilon_A = 0.0$ (open circle), 0.2 (solid circle), 0.4 (open square), 0.6 (solid square), 0.8 (open triangle), 1.0 (solid triangle), and 1.2 (open inversed triangle).

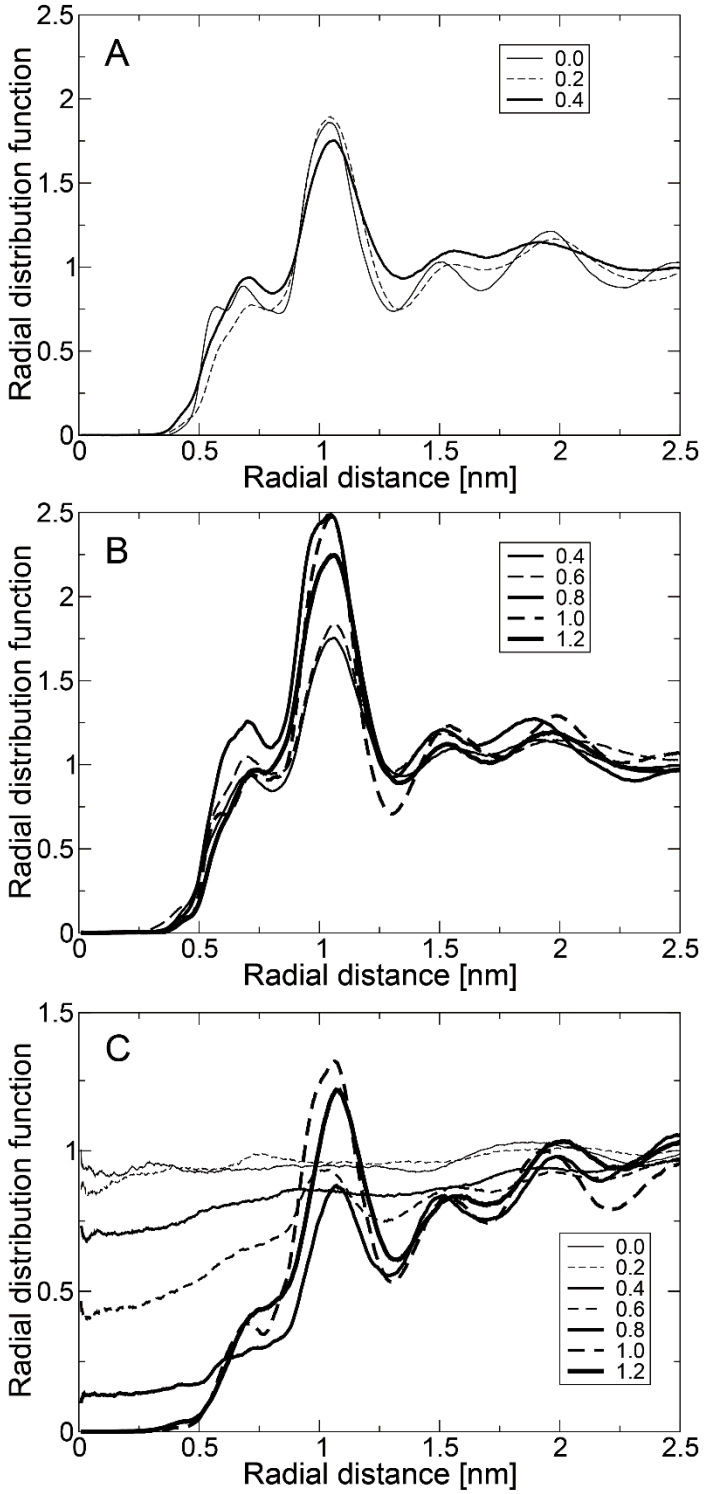

FIGURE 2.6 RDFs of C21 atoms of cholesterol molecules in the stretched bilayers for S40: (*A*) RDF calculated from the atoms within individual monolayer for the small areal strains, (*B*) RDF for the large areal strains (*B*), and (*C*) RDF calculated from the atoms between the upper and lower monolayers. The data for different areal strains are shown by different line types (see legend in the figure).

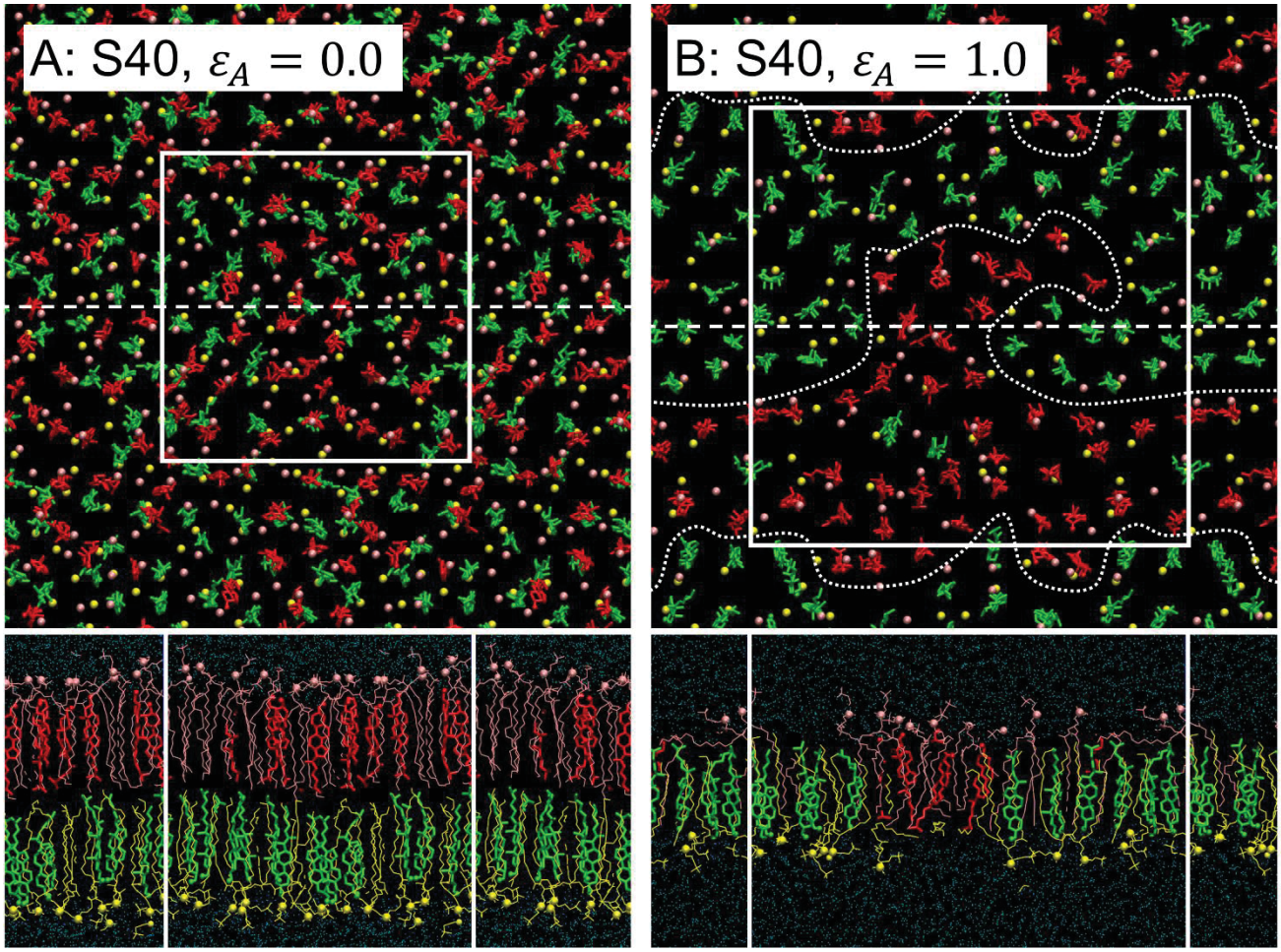

FIGURE 2.7 Representative snapshots of the stretched bilayers for S40 under areal strains of 0.0 (left) and 1.0 (right). The upper panels are top views and the lowers are side views of the systems cut along the dashed lines in the top views. Cholesterol molecules in the upper and lower monolayers are shown in red and green, respectively. DPPC molecules in the upper and lower monolayers are shown in pink and yellow, respectively. Phosphorous atoms in DPPC headgroups are shown as pink and yellow spheres. In the top views, water and DPPC molecules, except for the phosphorous atoms, are omitted for clarity. White lines in the top and side views show the outlines of the periodic simulation boxes. Dotted curves in the top-right figure represent the rough boundaries between the upper and lower component regions in the interdigitated bilayer.

2.4. DISCUSSION

2.4.1. Ordering Effect in Stretched Bilayers

Many studies have reported that cholesterol molecules increase the ordering of the hydrophobic chains of coexisting lipid molecules, the so-called ordering effect, in unstressed bilayers [43,44]. The

results here elucidate that the cholesterol ordering effect under stretching depends on the amount of cholesterol and the applied areal strain of the bilayer (see Fig. 2.4 *A*). In the low areal strain stage, the order parameter for each system monotonically decreases with increasing applied areal strain. In contrast, in the high areal strain stage, the order parameter increases with increasing applied areal strain, and this tendency is most prominent in the system with 40 mol% cholesterol. In the system with 40 mol% cholesterol, the two monolayers of the bilayer interpenetrate and form an interdigitated gel-phase-like structure (Fig. 2.7), especially under high areal strain. As the interdigitated gel-like structure is an ordered structure (Fig. 2.1 *C*), it might be less permeable to water molecules in the stretched bilayer, as in unstressed bilayers with different amounts of cholesterol [53]. Although more expensive calculations are required, the permeability change may be quantified by calculating the free energy profiles of water [54] across the stretched membranes. Because pore formation in the bilayer begins with penetration of water into the bilayer [31] (Fig. 2.1 *E*), the increase of the critical areal strain in phospholipid/cholesterol bilayers [8,15] (Fig. 2.3) seems to be due to the transient formation of the interdigitated gel-like structure.

2.4.2. Toughness of Red Blood Cell Membranes

The concentration of cholesterol in cell membranes differs depending on the type of cell: 20–30 mol% in typical animal cell membranes, 40–50 mol% in RBC membranes, and as high as 70 mol% in ocular lens membranes, whereas the amount of cholesterol is non-existent in coli bacillus membranes [1,55]. According to previous experimental studies [8], the elastic stiffness of the membrane, e.g., areal compressibility, monotonically increases with increasing cholesterol in this range (< 60 mol%). The simulations here have added evidence at the molecular level that a bilayer with 40 mol% cholesterol is the most resistant to pore formation, which causes the permeability increase and failure of the membrane. In regard to the toughness of the membrane, the feature may be favorable for red blood cells, because they require high elastic deformability and stability to pass through capillaries and are

exposed to high shear flows during blood circulation. Moreover, controlling the concentration of cholesterol in the membranes is a key factor in the development of synthetic RBCs to prevent hemolysis [56].

2.4.3. Stretch-Induced Interdigitation

In the findings in this chapter, the stretch-induced phase transition to the interdigitated gel-like phase in the cholesterol-containing bilayer is one of the most surprising discovery. According to experimental studies for lipid phase behaviors [57], excepting several lipid species e.g., 1,3-DPPC, F-DPPC, and dihexadecylphosphatidylcholine (DHPC), the interdigitation is known to occur only when bilayers are exposed to high hydrostatic pressure [58] or lower alcohols [59]. Furthermore, cholesterol is, interestingly, known to be an inhibitor of the pressure- and alcohol-induced interdigitation [60,61]. It might be one of the reason why the interdigitation is observed only in model phospholipid bilayers not in biological membranes, which usually containing cholesterol. Contrarily, although the mechanism of the stretch-induced interdigitation remains unclear, the MD simulations here provided a possibility of the stretch-induced interdigitation in cholesterol-containing bilayers (Figs. 2.1 and 2.7), which is a more realistic model for biological membranes than pure phospholipid bilayers. As the interdigitation is accompanied with drastic structural changes of the membrane, impacts of the interdigitation in biological membranes on the biological functions will be profound. This might be related to the biological responses to the mechanical stresses, i.e., cellular mechanotransduction.

2.5. SUMMARY

MD simulations of pore formation in stretched DPPC/cholesterol bilayers reveal that the critical areal strain, where the pore is formed, is influenced by the amount of cholesterol in the stretched bilayers. In particular, the critical areal strain reached a maximum when the amount of cholesterol was 40 mol%. With increasing the areal strain of the bilayer, the lipid tails become disordered and the tilt

angle of the cholesterol molecules increases, resulting in the formation of a hydrophilic pore. However, especially in the system with 40 mol% cholesterol, interdigitation of lipid and cholesterol molecules is observed at high areal strain, resulting in increased ordering of the lipid tails and the formation of a hydrophobic pore. The transient formation of the interdigitated gel-phase-like structure in the stretched phospholipid/cholesterol bilayer might increase the resistance to water permeability, followed by the increase of the critical areal strain.

CHAPTER 3.
CHOLESTEROL EFFECTS ON LINE TENSION OF PORE EDGE IN PHOSPHOLIPID/CHOLESTEROL BILAYER

3.1. INTRODUCTION

A formation of water-filled pores penetrating the bilayer is an initiation of the bilayer rupture. Depending on the intensity of mechanical stress on the bilayer, the pore can spontaneously close or continue to grow. The excessive growth of the pore disturbs the cellular environments and induces rupture of the bilayer. On the positive aspects, the pore in the bilayer acts as a path into the cell for extracellular molecules and enables passive molecular transport. The temporal permeabilization with the pore formation has been used as artificial molecular transport techniques, such as electroporation [16] and sonoporation [62–64]. To prevent the unexpected bilayer rupture and develop the effective molecular transport techniques, it is necessary to understand the details of pore dynamics in the bilayer under mechanical stresses.

Previously, to describe the pore dynamics, Litster proposed the free energy difference ΔF between bilayers with and without a pore with a radius R, as:

$$\Delta F = 2\pi\gamma_L R - \pi\gamma_S R^2 , \tag{3.1}$$

where γ_L and γ_S are the line tension (edge tension) and the surface tension, respectively [25]. This model describes the free energy change with the change of the pore radius as the balance between the edge energy of the pore and the surface energy of the bilayer. From this model, the pore spontaneously closes when the pore radius is below $R_C = \gamma_L/\gamma_S$, which is defined as the critical pore radius. However, when the pore exceeds R_C, the pore spontaneously grows, resulting in the rupture of the bilayer. Thus,

the line tension γ_L, which governs R_C, is an important property of the bilayer and is useful for discussing the bilayer-edge-related phenomena, that is, rupture.

The estimations of the line tension have been conducted by experimental [65–67], theoretical [68], and computational studies [29,51,69]. In these experiments, researchers have estimated the line tension from the pore closure dynamics in giant bilayer vesicles under stresses. These studies reported that the line tension depends on not only the lipid composition of the bilayer but also the purity of the lipids [66]. In computational studies, MD simulations of planar bilayer systems with a pore [29] or bilayer ribbon system [69] have been performed. These studies clarified that the molecular details of the bilayer edge structure, and the line tensions estimated in MD simulations (10−50 pN) are in qualitative agreement with those obtained from experiments (5−30 pN). In these MD simulation studies, pure phospholipid bilayers or mixture bilayers of phospholipids, which have different lengths of the hydrophobic tails [70,71], were used.

Actual cell membranes are intricately composed of various molecules. Among the various molecules in the cell membranes, cholesterol is especially known to be of importance. Cholesterol is abundant in mammalian cell membranes and the cholesterol concentration in phospholipid bilayers strongly depends on the type of the cell [1]. The cholesterol concentration is closely related with various properties of the bilayer. In particular, experimental studies reported that the inclusion of cholesterol into the bilayer altered the line tension of the bilayer [65,66]. Nevertheless, the details of the edge structure of cholesterol-containing bilayers at the molecular level and the relationship between the cholesterol around the pore edge and the line tension are still unclear. Furthermore, the edge structures at the molecular level are potentially related to the translocations of phospholipids between the inner and the outer leaflet of the bilayer [72] and the permeations of ions and peptides trapped on the bilayer surface [73,74]. Thus, the molecular-level structure of the pore edge in the cholesterol-containing bilayer, which is a more realistic model for biological cell membranes than a pure bilayer, is a meaningful research target.

In this chapter, to understand the cholesterol effects on the pore dynamics, MD simulations of phospholipid/cholesterol bilayers with a pore under constant bilayer area conditions are performed and the line tension of the cholesterol-containing bilayer is estimated. The line tension is calculated from the free energy model of a bilayer with a pore proposed by Tolpekina and co-workers [29]. In their model, the line tension can be estimated from the critical condition that a pore spontaneously closes. Additionally, the potential relationships between the line tension of the bilayers and the efficiency of the pore-mediated molecular transport into cells are presented.

3.2. METHOD

3.2.1. Estimation of Line Tension

The line tension of the pore edge is estimated from MD simulations. For this purpose, the method presented by Tolpekina et al. [29] is applied to the DPPC/cholesterol bilayer systems. In this method, to include the finite constant area in MD simulations, the free energy of the bilayer with a pore can be determined by:

$$F = 2\pi\gamma_L R + \frac{K_A}{2A_0}\left(\varepsilon_A A_0 - \pi R^2\right)^2, \tag{3.2}$$

where K_A is the area compressibility modulus [29]. As defined in the Chapter 2, ε_A is the areal strain of the simulation box area calculated by $A_{||}/A_0 - 1$. A_0 is the simulation box area without a pore at equilibrium. Here, we consider the equation $dF/dR = 0$, whose roots are the stable or quasi-stable pore radii. When the discriminant of the cubic equation is negative, the equation has no positive root, which means that a pore will spontaneously close. The critical condition is given by:

$$\varepsilon_{pc} = 3\left(\frac{\gamma_L}{2K_A}\right)^{\frac{2}{3}}\left(\frac{\pi}{A_0}\right)^{\frac{1}{3}}, \tag{3.3}$$

where ε_{pc} is the critical pore closure areal strain where a pore spontaneously closes. Equation (3.3) is rewritten as:

$$\gamma_L = 2K_A\left(\frac{\varepsilon_{pc}^3 A_0}{27\pi}\right)^{\frac{1}{2}}. \tag{3.4}$$

K_A and A_0 can be obtained from MD simulation of the bilayers without a pore at equilibrium. The pore closure areal strain ε_{pc}, where a pore is closed, is estimated by equilibrating MD simulations of stretched bilayers with a pore under various areal strain conditions. From these three parameters obtained in MD simulations and Eq. (3.4), the line tension can be estimated.

Bilayers with a pore are prepared through equibiaxial stretching simulations of intact bilayers. Stretch-induced pore formation was proposed to be more suitable for the purpose here, the investigation of pore dynamics under mechanical stresses, than several other protocols used for making a pore employed in previous studies, such as self-aggregation [75] and manual construction [29,69]. However, it is noted that the pore structures are very similar despite the different protocols used for the pore formation [76]. Thus, the selection of the protocols is expected to be a minor problem unless the pore formation process itself is discussed.

3.2.2. Initial Systems

One pure DPPC bilayer system and two DPPC/cholesterol bilayer systems are used, as the force field and simulation protocols of DPPC bilayers have been well studied in MD simulations. These bilayers are composed of 200 DPPC and cholesterol molecules so that the cholesterol concentrations are 0, 20, and 40 mol%, respectively. These bilayers are set in the center of a square cylinder simulation box with periodic boundary conditions. The systems are solvated in at least 8284 water molecules. DPPC, cholesterol, and water molecules are represented by the united atom force fields for DPPC [36], for cholesterol [37], and the simple point charge model for water [38]. The initial configurations of bilayers are taken from the previous study [77]. The systems were equilibrated at a temperature of 323 K and a pressure of 0.1 MPa for at least 100 ns in the previous study [77]. The trajectories during the latter 50 ns are used for the analysis of the bilayers at equilibrium. Details of MD simulation parameters

are summarized in the supplementary material of the previous study [77] and the same parameters are used in the current investigation.

3.2.3. MD Simulation Outline

To obtain the line tension γ_L from Eq. (3.4), the pore closure areal strain ε_{pc}, where a pore spontaneously closes, is estimated from the results of a series of MD simulations of bilayers with a pore. Herein, MD simulations are divided into three stages: stretching, compressing, and equilibrating stages (Fig. 3.1). The first stage is to induce the pore formation, the second is to modulate the applied areal strain of the system with a pore, and the third is to examine whether the pore closes under the constant areal strain conditions. Through these stages, MD simulations of the bilayers are performed with a thermostat [78] and barostat (Berendsen et al., 1984) to maintain the temperatures of DPPC, cholesterol, and water molecules at 323 K and the pressure in the z-direction (normal to the bilayer) at 0.1 MPa. For the x- and y-directions (bilayer plane), the box lengths are controlled to apply an arbitrary areal strain on the bilayer. The box lengths are elongated or shortened at a constant rate c, and, simultaneously, the atom positions are proportionally scaled to follow the changes of the box lengths [32]. c is set to a positive value for stretching, negative for compressing, and zero for maintaining the bilayer area at a constant level.

In the stretching stage, the bilayer systems without a pore at equilibrium, taken from the previous study [77], are used for the initial configurations of this stage. Using these systems, MD simulations with c = 1.0 m/s are performed until a pore is formed. It should be noted that, to induce the pore formation in conventional MD simulations, the bilayers have to be excessively stretched. This is believed to be because there is an energetic barrier between the bilayer with and without a pore [79], which impedes the transition of the bilayer state from “without a pore” to “with a pore”. In the MD simulations here, the pore formation occurs in the range of the areal strain from about 1 to 2. The range is considerably larger than the pore closure areal strain ε_{pc}, where a pore spontaneously closes (< 0.5).

In the compressing stage, the stretched bilayer with a pore just after the pore formation in the stretching stage is used for the initial configuration of this stage. To relax the excessive areal strain on the bilayer, MD simulations with $c = -1.0$ m/s are performed until the areal strain reaches 0. As both the stretching and compressing stages occur at non-equilibrium, the bilayer system in the two stages has not yet reached a stable state nor a quasi-stable state.

In the equilibrating stage, MD simulations with $c = 0$ m/s are performed for 100 ns. The initial configuration of this stage is obtained from the trajectories in the compressing stage, where the box area is set to satisfy areal strains $\varepsilon_A = 0.1$, 0.2, 0.3, 0.4, 0.5, and 0.6. After the 100-ns simulation in the equilibrating stage, the existence of the pore is examined by visual inspection and the minimum areal strain where a pore remains in the bilayer and the maximum areal strain where a pore is no longer observed are obtained. The ε_{pc}, where a pore spontaneously closes, is expected to be in the range between the two areal strains. Accordingly, the upper and lower limits of the line tension are estimated by Eq (3.4).

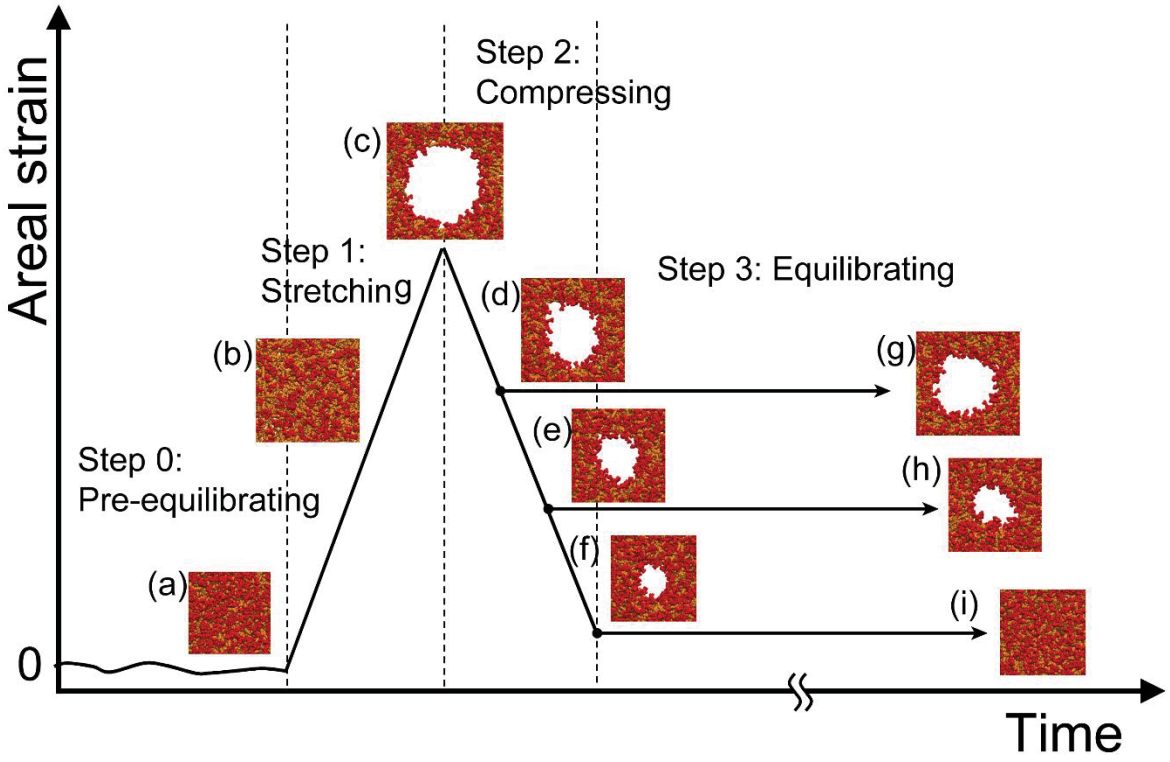

FIGURE 3.1 Schematic of the outline of MD simulations of the pore formation and closure. Panels (*a–i*) are representative snapshots of the pure DPPC bilayer during stretching, compressing, and equilibrating stages. White regions in panels (*c–h*) are pores.

3.2.4. Analysis

In the bilayer without a pore, the bilayer area is considered to be equal to the simulation box area A. The area compressibility modulus of the bilayer K_A is estimated from the fluctuations of $A_{||}$ at equilibrium by using:

$$K_A = \frac{A_0 k_B T}{\sigma_A^2}, \tag{3.5}$$

where σ_A^2 is the variance of $A_{||}$, k_B is the Boltzmann constant, and T is the temperature of the system. For the estimation of K_A, the trajectories in the pre-equilibrating stage obtained from the previous study [77] are used.

As there are large fluctuations of the geometric structure of the pore in MD simulations, it is

difficult to clearly distinguish the pore edge region of the bilayer. Herein, the region of the pore edge is defined by using the distance from the bilayer center along the *z* axis (normal to the bilayer). The bilayer center is defined as the center of mass of the phosphorous atoms in DPPC molecules and the pore edge is defined as the region within which the distance is lower than 0.8 nm (region between the two dashed white lines in Fig. 3.4). A DPPC molecule, whose phosphorous atom is in the pore edge region, is considered to be in the pore edge region. As with the DPPC molecule, a cholesterol molecule is distinguished by the position of the hydrogen atom in the hydroxyl group.

3.3. RESULTS

3.3.1. Pore Formation and Closure

In the stretching stage, owing to the stretching of the bilayer, the bilayer area increases and a pore is formed when the areal strain exceeds a critical value (Fig. 3.1 (*a*–*c*)). The pore rapidly grows to a constant area, which depends on the applied areal strain (Fig. 3.1 (*c*)). After the pore formation, the simulation proceeds to the compressing stage. In the compressing stage, owing to the compression, the area of the pore decreases; however, the pore is not closed only when the areal strain ε_A reaches 0.0 (Fig. 3.1 (*c*–*f*)). In the equilibrating stage, under lower areal strains, the area of the pore decreases gradually during the 100-ns equilibrium simulations, which resulted in the pore closure (Fig. 3.1 (*f*) and (*i*)). However, under higher areal strains, the pore closure does not occur at least within the current simulation time (Fig. 3.1 (*d*), (*e*), (*g*), and (*h*)). Figure 3.2 shows the snapshots of DPPC and DPPC/cholesterol bilayers taken from the end of the equilibrating stage. In the pure DPPC bilayer, the pore closure occurs with the areal strains $\varepsilon_A \leq 0.1$, and does not occur for $\varepsilon_A \geq 0.2$ (upper row in Fig. 3.2). In the DPPC bilayer with 20 and 40 mol% cholesterol, the pore closure occurs for $\varepsilon_A \leq 0.2$ and 0.3, and does not for $\varepsilon_A \geq 0.3$ and 0.4, respectively (middle and lower rows in Fig. 3.2). These indicate that ε_{pc}s for the bilayers are expected to be in the range of 0.1–0.2, 0.2–0.3, and 0.3–0.4, respectively, and ε_{pc} increases with the increase of the cholesterol concentration (Fig. 3.3 *A*).

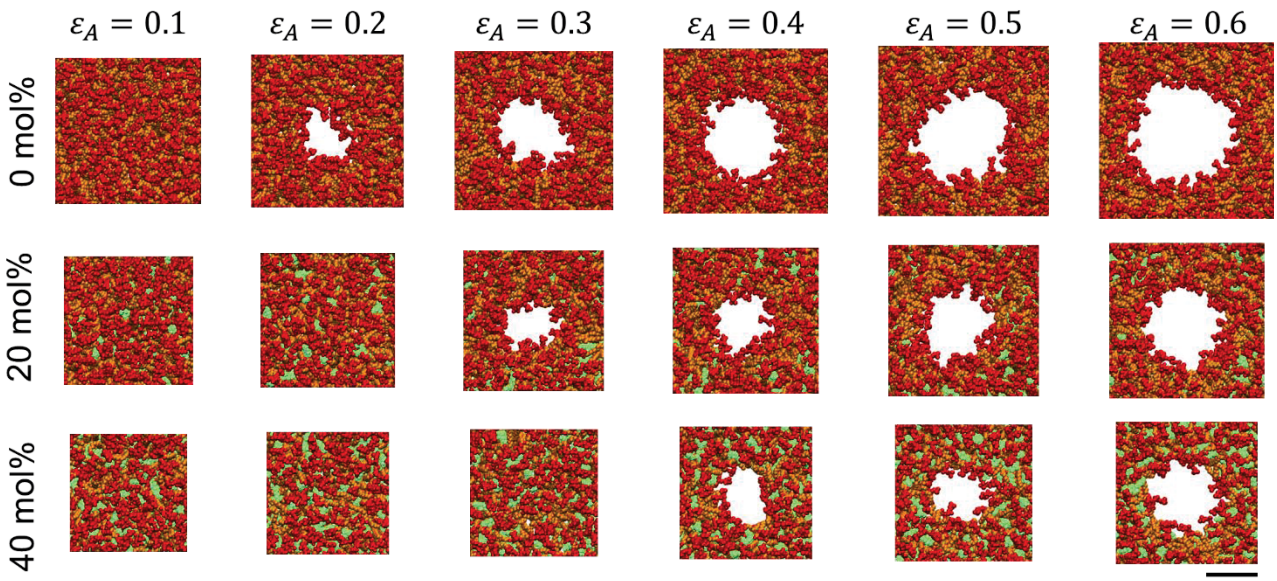

FIGURE 3.2 Representative snapshots of the bilayers containing cholesterol molecules at 0 (upper low), 20 (middle), and 40 mol% (lower) after stretching, compressing, and equilibrating MD simulations. The column of the panels corresponds to the applied areal strain. DPPC head groups are shown in red, DPPC tails in orange, and cholesterol molecules in light green. Water molecules are not shown for clarity. White region at the center of the panels is a pore. The black bar on the bottom right corner corresponds to 3 nm.

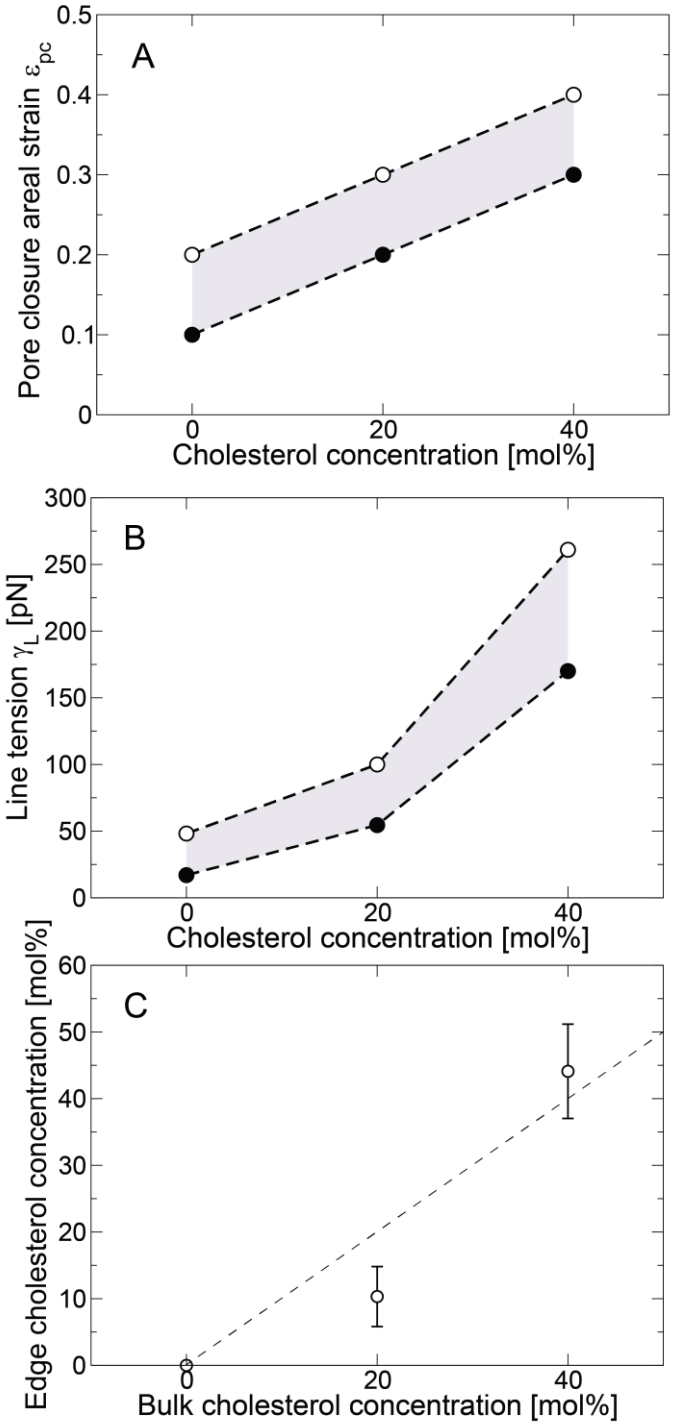

FIGURE 3.3 Relationships between cholesterol concentration and critical areal strain (*A*), line tension (*B*), or cholesterol concentration in the pore edge region (*C*). The dashed lines show the linearly interpolated lines between the points, and the region, where the real critical areal strain and the line tension are expected to be found, are shown in gray. Black bars in the panels *A* and *B* represent the estimated range within which are the critical areal strain or the line tension. Error bars in the panel *C* represent standard deviation.

3.3.2. Estimation of Line Tension

From the trajectory of the bilayer at equilibrium taken from the previous study [77], the averaged system box areas on the *x*-*y* plain A_0 are 65.4, 48.7, and 39.2 nm^2 for the bilayers containing cholesterol at 0, 20, and 40 mol%, respectively. The corresponding areas per molecule are 0.65, 0.49, and 0.39 nm^2, respectively, which are in good agreement with those obtained from MD simulations reported by other groups [42,54]. Additionally, the variances of $A_{||}$, σ_A^2, are 0.95, 0.54, and 0.23 nm^4 for the different cholesterol concentration bilayers, respectively. From A_0, σ_A^2, and Eq. (3.5), the area compressibility modulus K_A can be calculated as 306, 402, and 760 mN/m, respectively. K_A increases with the increase of the cholesterol concentration, which is in qualitative agreement with that observed from experiments [8,80]. Using these parameters A_0, K_A, and ε_{pc} in Fig. 3.3 *A*, the line tension γ_L can be calculated by Eq. (3.4) and the relationships between the line tension and the cholesterol rate are shown in Fig. 3.3 *B*. The upper and lower limits of the line tensions of the bilayers containing cholesterol at 0, 20, and 40 mol% are estimated to be 17.0–48.2, 54.5–100, and 170–261 pN, respectively. The line tension of the pure DPPC bilayer is in agreement with those estimated by different methods in previous MD simulation studies (27.5–50 pN) [51,69,75]. The line tension increases with the increase of the cholesterol concentration, which qualitatively agrees with those for similar phospholipid bilayers reported from experiments [65,66].

3.3.3. Pore Edge Structure

Figure 3.4 shows the representative snapshots of the bilayers with stable pores, whose radii are similar. From a visual inspection, the pore edges are lined with a considerable number of DPPC molecules and several cholesterol molecules. The number of cholesterol molecules in the pore edge region increases with the increase of the cholesterol concentration in the whole system. Figure 3.3 *C* shows the relationship between the cholesterol concentration in the pore edge region and that in the

whole system. In the bilayer with 20 mol% cholesterol, the edge cholesterol concentration is slightly lower than the cholesterol concentration of the whole system. However, in the bilayer with 40 mol% cholesterol, the edge cholesterol concentration is slightly higher.

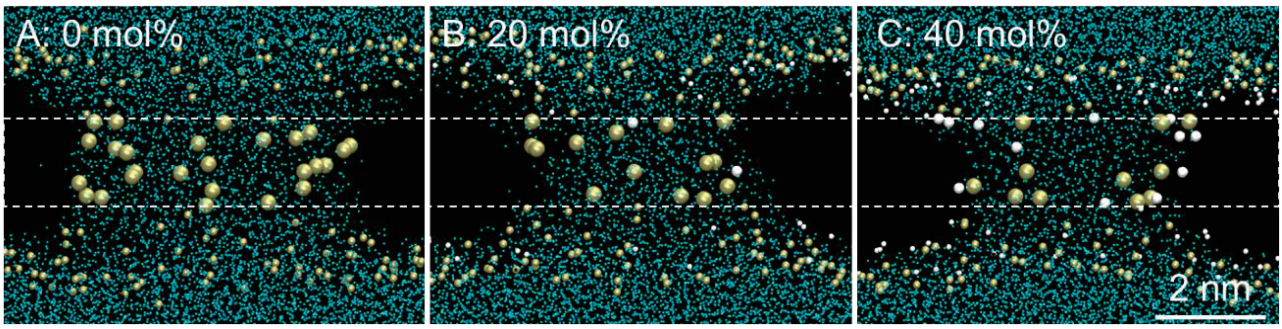

FIGURE3.4 Representative snapshots of the pore structures in the bilayer containing cholesterol at 0 (*A*), 20 (*B*), and 40 mol% (*C*). Phosphorus atoms of DPPC molecules are shown as tan beads, hydrogen atoms of cholesterol molecules as white beads, and water molecules are blue. Dashed lines show the boundary between the pore edge region and the others. Phosphorous atoms and hydrogen atoms of cholesterol molecules in the pore edge region are enlarged for clarity.

3.4. DISCUSSION

3.4.1. Cholesterol Effects on Line Tension

From the simulation here, the line tension increases with the increase of the cholesterol rate (Fig. 3.3 *B*). First, the results here are compared with the experimental data. However, experimental data of the line tension in DPPC bilayers are non-existent to my knowledge, whereas DPPC bilayers are commonly used in MD simulation studies. Thus, experimental data for similar phospholipids are used to evaluate the cholesterol effects obtained in the MD simulation here. In experimental studies, similar phospholipid molecules, for example, stearoyloleoylphosphatidylcholine (SOPC) or dioleoylphosphatidylcholine (DOPC), are used and the line tensions of pure DOPC bilayers are in the range of 3.9–27.7 pN (summarized by Portet and Dimova [67]). Zhelev and Needham reported that the line tension of pure SOPC bilayers is increased about 3-fold by the inclusion of cholesterol at 50 mol% [65]. Karatekin and co-workers also reported that the line tension of pure DOPC bilayers is

increased about 3-fold by the inclusion of cholesterol at 30 mol% [66]. In the MD simulations here, the line tension of the pure DPPC bilayer is increased about 3- to 15-fold by the inclusion of cholesterol at 40 mol% (Fig. 3.3 *B*). Cholesterol effects on the line tension of the DPPC bilayer in the MD simulation here are large compared to those observed for similar phospholipid bilayers investigated experimentally. This difference can be considered to be acceptable because of the large variations in experimental measurements [67] and the underlying effects of the types of phospholipids, which are difficult to state from the available data. This paper is, to the best of my knowledge, the first estimation of the line tension in the cholesterol-containing bilayer on the molecular scale and succeeds in determining the relationship between the cholesterol concentration and the line tension.

The line tension of the pore edge, which is an energetic loss per edge length, partially arises from the bending energy of the phospholipid monolayer of the bilayer around the pore edge [51]. Although estimation of the bending modulus at the nanometer edge is a challenging problem [81], the increase of the cholesterol concentration around the pore edge might increase the bending modulus of the pore edge and the line tension [82]. According to previous experimental [83] and simulation studies [9], cholesterol molecules rectify the disordered orientations of hydrophobic tails of co-existing phospholipid molecules, which is one of the causes for the high bending moduli of cholesterol-containing bilayers. In the MD simulations here, the cholesterol molecules are distributed around the pore edge (Fig. 3.4) and the cholesterol concentration around the pore edge increases with the increase of the overall cholesterol concentration (Fig. 3.3 *C*). Thus, the increase of the cholesterol concentration around the pore edge might increase the bending modulus of the pore edge and the line tension.

3.4.2. Line Tension and Physical Methods for Drug Delivery

It is known that the cholesterol concentration varies depending strongly on the type of cell [1]. With the increase of the cholesterol concentration, the line tension can increase about 3–15 fold in the MD simulation (Fig. 3.3 *B*). From Lister's model for pore dynamics [25], an increase of the line tension

means an increase of the critical pore radius R_C (= γ_L/γ_S). It is known that the tension of the bilayer also depends on the cholesterol concentration. For example, it is reported that the tension of a phospholipid bilayer containing cholesterol at 40 mol% is about 2–3 times larger than that of a pure bilayer [84]. In this case, bilayers containing cholesterol at 40 mol% can contain 1–7.5 times larger pores. Additionally, the pore closure process with the higher line tension is faster owing to the higher energetic loss to maintain the edge [66]. In the physical methods of molecular transport through the pore, for example, sonoporation, these significant differences of the line tension and the critical pore radius R_C might limit the size and the amount of transporting molecules without rupture of the bilayer. In fact, the transduction efficiencies by sonoporation treatment are different depending on the cell lines [85]. Although the transduction efficiency is sensitively affected by a huge number of potential factors [62], the line tension, which depends strongly on the membrane composition, especially cholesterol concentration, might be the underlying factor and will be useful for explaining the variation of the transduction efficiencies in sonoporation. However, it should be noted that real biological membranes are consisted of various lipids, mostly of unsaturated lipids. The bending rigidity of mono-unsaturated lipid bilayer, e.g. SOPC [82], increases with the cholesterol concentration, as of saturated phospholipid bilayer, e.g. dimyristoylphosphatidylcholine [86].

3.5. SUMMARY

To understand the cholesterol effects on the line tension of the pore edge and the molecular details of the pore edge structure, MD simulations of DPPC/cholesterol bilayers with a pore were performed. The pores in the cholesterol-containing bilayers are lined with not only the DPPC molecules but also the cholesterol molecules. The cholesterol concentration in the pore edge region is almost the same as the cholesterol concentration in the whole system. Based on the free energy model of the bilayer with a pore, the line tension of the pore edge is estimated to considerably increase with the increase of the cholesterol concentration. The increasing tendency is in agreement with that observed from

experiments. The increase of the line tension might arise from the increase of the bending rigidity of the bilayer around the pore edge, which is induced by the cholesterol molecules distributed around the pore edge. Additionally, the considerable difference of the line tension, depending on the bilayer compositions, might be useful to explain the large variations of the transduction efficiency observed with sonoporation treatment.

CHAPTER 4.
EFFECTS OF STRETCHING SPEED ON PORE FORMATION IN PHOSPHOLIPID/CHOLESTEROL BILAYER UNDER MECHANICAL STRESSES

4.1. INTRODUCTION

To understand the details of mechanical rupture, many biomechanical experiments have been conducted on biological cell membranes [87–92] and model membranes consisting of phospholipid bilayers [8,22,23,53]. Under static or at least quasistatic stresses, the rupture tension of biological membranes varies in the range from 1 to 30 mN/m and the rupture areal strain in the range from 0.01 to 0.05 depending on the lipid composition. In addition to the lipid composition, the time history of the applied stress or strain affects the rupture stress or strain. Evans and coworkers [23] performed micropipette aspiration experiments at various loading rates (0.01–100 mN/m/s) and showed that the rupture tension of vesicles increased with increasing loading rate. The rupture tension for a pure SOPC vesicle, for example, increased 2-fold when the loading rate increased by 3 orders of magnitude [23]. Li and coworkers [89,93] performed impulse-like stretching experiments on RBCs using a laser-induced cavitation. In their experiments [89,93], the RBCs were rapidly stretched within tens of microseconds and could withstand much higher areal strains of about 0.3, which is about one order of magnitude higher than those in quasistatic stretching experiments. These experiments indicate that membrane rupture is a time-dependent phenomenon and information on the rate, at which a membrane is stressed, is essential to understanding membrane rupture. However, the molecular details of the initiation of the rupture, pore formation, are still unclear.

Many researchers, including our group, have performed MD simulations of the pore formation in

the bilayer under various conditions [29,31,32,77,94,95]. Our group has performed MD simulations of stretched phospholipid bilayers and investigated the effects of stretching speed [32] and cholesterol concentration [77] on pore formation. For pure phospholipid bilayers, the critical areal strain, where a pore is formed, increases with increasing stretching speed, while that under quasistatic stretching also increases with the increasing cholesterol concentration up to 40 mol%. In the simulations, a phospholipid bilayer containing cholesterol at 40 mol% under quasistatic stretching is the toughest composition and forms an interdigitated gel-phase-like structure, in which phospholipid and cholesterol molecules in one leaflet of the bilayer penetrate into the opposite leaflet and become ordered, under stretching. The stretch-induced interdigitation might retard pore formation and enhance the toughness of the phospholipid/cholesterol bilayer [77]. Although stretch-induced interdigitation has been also observed in some coarse-grained simulations of pure bilayers under tension [96,97], the details of that system are still unknown.

Mammalian cell membranes are usually rich in cholesterol molecules within the phospholipid bilayer [1]. The inclusion of cholesterol in the phospholipid bilayer alters various bilayer characteristics. Thus, consideration of the effects of cholesterol at a molecular level is essential to understanding pore formation and subsequent bilayer rupture. Additionally, whereas it has been shown that the stretching speed markedly affects pore formation in a pure phospholipid bilayer, the mechanisms behind the stretching speed effects seen in cholesterol-containing bilayer are still unknown at the molecular level. In particular, the dependence of the stretch-induced interdigitation on the stretching speed must be clarified to understand pore formation under unsteady stretching conditions.

In this chapter, a series of molecular dynamics simulations of a DPPC bilayer comprising cholesterol molecules at 40 mol% and a pure DPPC bilayer for comparison under stretching at various stretching speeds is performed. The effects of stretching speed on pore formation in the DPPC/cholesterol bilayer are evaluated by analyzing the pore formation patterns, molecular

orientations under stretching, critical areal strain where the pore is formed, bilayer thickness, and phase transition to interdigitated gel-like phase under stretching.

4.2. METHODS

4.2.1. Bilayer Systems

A planar DPPC/cholesterol bilayer system with a cholesterol concentration of 40 mol% and a pure DPPC bilayer system for comparison were employed. For fair comparison of the stretching speed and to minimize the effects of system size differences between the two systems on the pore formation [29], the total number of DPPC and cholesterol molecules in the DPPC/cholesterol bilayer was carefully set to minimize the difference in bilayer areas between the pure DPPC and DPPC/cholesterol bilayers at equilibrium states at 323 K and 1 bar. In this study, the pure DPPC and DPPC/cholesterol bilayers were respectively composed of 128 DPPC and 16,483 water molecules, and 128 DPPC, 86 cholesterol, and 13,842 water molecules, in a square cylinder simulation box with periodic boundary conditions. Here, the number of water molecules was set to prevent the interactions between periodic images of bilayer in the *z*-direction during stretching [32]. DPPC and cholesterol molecules were represented by the united atom force fields for DPPC [36], and cholesterol [37] and water molecules by a simple point charge model [38]. For equilibration, constant temperature (T) and pressure (P) MD simulations were performed for more than 100 ns at 323 K and 1 bar. The areas of the pure DPPC and DPPC/cholesterol bilayers in the equilibrium states were 41.98 and 41.84 nm^2, respectively, which were essentially as expected. Several structural properties of the pure DPPC and DPPC/cholesterol bilayers in equilibrium states were in agreement with those obtained experimentally [10,39,83,98] and in other simulations [54]. The details of the construction of the systems, MD simulation parameters for the equilibrium simulation, and the structural properties of the bilayers in equilibrium states are summarized in the Appendix A2.

4.2.2. Unsteady Stretching Simulation

The following method [32] was employed for unsteady stretching (US) of the bilayer, involving proportional and temporal scaling of both the atom positions and system box lengths, implemented in GROMACS codes as the deform option. Briefly, the box lengths l_i and coordinates of all atoms r were proportionally scaled per time step Δt from l_i to μl_i and r to μr with

$$\mu = 1 + \frac{c}{l_i}\Delta t \tag{4.1}$$

($i = x, y, z$), where c is the stretching speed, c set to eight values in the range from 0.025 to 30 m/s. Although the stretching speeds here were specified at much higher values than those used during micropipette experiments [23], these values were chosen because of computational limitations. For example, it took about 3,800 CPU hours on a Linux cluster with 2.21 GHz Opteron processors to complete a simulation for a DPPC/cholesterol bilayer with c = 0.05 m/s. The same value of μ in the x and y directions were used to express the equibiaxial stretching. However, to maintain the pressure in the z direction at a constant value, Berendsen's scaling factor [49],

$$\mu = 1 - \frac{\beta \Delta t}{3\tau_p}\{P_0 - P(t)\} \tag{4.2}$$

where τ_p = 0.5 ps, $\beta = 4.5 \times 10^{-5}$ bar^{-1}, and P_0 = 1 bar, was applied for scaling in the z direction.

During stretching, each temperature for DPPC, cholesterol, and water was individually kept constant at 323 K using the velocity rescaling method [78] with a 0.2-ps coupling constant. The simulation parameters of the US simulation were essentially the same as those for the equilibrium simulations (see Appendix A2) except for the update frequency of the neighbor list (every 10 steps for $c < 1.0$ m/s and every step for $c \geq 1.0$ m/s). To validate the parameters in the US simulations, the same simulations were performed using different parameters: calculation precision (single or double precision), coupling constant τ_p for Berendsen's scaling factor (0.3–1.0 ps), or number of water molecules (13,842 or 26,183 water molecules). The essential pore formation process was independent of the parameters mentioned above. Because of the statistical nature of pore formation [95], several

replicates of the US simulations, starting from different initial configurations, were performed to obtain sample averages. The number of the replicates for the stretching speed conditions is summarized in Table 4.1.

TABLE 4.1 Summary of parameters for the US simulations

Label	Replicates	Stretching speed [m/s]	ε_c mean ± S.D.	Multi-pore rate
DC0.025	3	0.025	1.43 ± 0.04	0.00
DC0.05	5	0.05	1.57 ± 0.12	0.00
DC0.30	6	0.30	1.66 ± 0.18	0.00
DC1.00	20	1.00	1.57 ± 0.18	0.20
DC3.00	20	3.00	1.56 ± 0.23	0.65
DC10.0	20	10.0	1.67 ± 0.22	0.90
DC30.0	20	30.0	1.87 ± 0.33	1.00
PD0.025	3	0.025	0.91 ± 0.04	0.00
PD0.05	5	0.05	0.88 ± 0.08	0.00
PD0.30	6	0.30	1.05 ± 0.10	0.50
PD1.00	20	1.00	1.14 ± 0.12	0.55
PD3.00	20	3.00	1.24 ± 0.15	0.85
PD10.0	20	10.0	1.37 ± 0.15	0.95
PD30.0	20	30.0	1.48 ± 0.14	1.00

4.2.3. Quasistatic Stretching Simulation

For comparison with the US simulations, a series of constant $NP_zA_{\|}T$ MD (quasistatic stretching, QS) simulations of the bilayers [32,48,77] were performed at constant temperature T = 323 K, pressure in the z direction P_z = 1 bar, and various constant bilayer areas $A_{\|}$ that were set to satisfy areal strains up to 1.40, as explained below. The initial configurations were extracted from the trajectories of the US simulations with c = 0.05 m/s and performed the simulations using these systems for at least 100 ns so that the systems were equilibrated. The simulations were performed starting from three initial configurations, around the critical areal strains where a pore is formed. The basic QS simulation

protocols were same to that of the stretching simulation in the Chapter 2.

4.2.4. Analysis

The lengths of the simulation box became l_x, l_y, l_z, and the bilayer thickness l_t upon stretching. The l_t was defined as the distance between phosphorous atoms of DPPC molecules in the upper and lower layers. The bilayer area in the system $A_{\parallel}$ was defined as $A_{\parallel} = l_x \times l_y = l_x^2$ for $l_x = l_y$ in equibiaxial stretching. The areal strain of the bilayer ε_A was also defined as $\varepsilon_A = (l_x/l_{x0})^2 - 1$, where l_{x0} is the average value of l_x during the latter 50 ns of the equilibrium simulation. Ordering in the hydrophobic tails of lipid molecules in the US simulations was evaluated by the averaged instantaneous order parameter $\hat{S}_{CD}$ [99],

$$\hat{S}_{CD} = -\frac{1}{2}\hat{S}_{zz} = -\frac{1}{2}\left(\frac{1}{N_C}\sum_{i=1}^{N_C}\frac{1}{2}\left(3\cos^2\Theta_i - 1\right)\right), \tag{4.3}$$

where Θ_i is the angle between the axis of the ith molecular axis and bilayer normal (the z axis) and N_c is the number of carbons in the lipid chains. In this study, the number of carbons in *sn*-2 chains was used (N_c = 14). For the QS simulation, $\hat{S}_{CD}$ was averaged over time, which is same to $\overline{S}_{CD}$ defined by the Eq. (2.1) in the Chapter 2. Furthermore, to analyze the orientations of cholesterol molecules during both the stretching simulations, the cholesterol tilt angle θ_c was defined as the instantaneous angle between the vector linking the C5 and C21 carbon atoms in the cholesterol ring structure and the bilayer normal (the z axis). The C5 and C21 atoms are hydrocarbon atoms that both belong to the steroid ring of the cholesterol molecules and are bonded to the oxygen atom of the hydroxyl group and the hydrocarbon chain, respectively.

In the previous QS simulation in the Chapter 2 ([77]), the stretch-induced transition to the interdigitated gel-phase-like structure of the DPPC bilayer containing cholesterol at 40 mol% is likely to be completed around ε_A = 1.00 through maximization of $-\hat{S}_{CD}$. However, such a transition is not observed in pure DPPC bilayers. The DPPC/cholesterol bilayer under ε_A = 1.00 was assumed to form

a standard interdigitated gel-like bilayer, and the pure DPPC bilayer was assumed not to form an interdigitated gel-like bilayer structure under stretching, at least compared with the DPPC/cholesterol bilayer. Based on these assumptions, an evaluation index for the transition to the interdigitated gel-like phase R_{Li} was defined as $R_{Li}(c) = \left(\hat{S}_{Li}^{chol}(c) - \hat{S}_{Li}^{pure}(c)\right) / \left(\hat{S}_{Li}^{chol}(qs) - \hat{S}_{Li}^{pure}(c)\right)$. $\hat{S}_{Li}^{chol}(c)$ and $\hat{S}_{Li}^{pure}(c)$ are the order parameter $\hat{S}_{CD}$ of, respectively, the DPPC/cholesterol and pure DPPC bilayers, where the bilayer thicknesses becomes congruent with that for the DPPC/cholesterol bilayer under ε_A = 1.00. R_{Li} will take on a value close to 1 when the bilayer forms an interdigitated gel-phase-like structure and will be around 0 when the bilayer dose not, as is the case for the pure DPPC bilayer. Note that the overlap length of the lipid tails that is a measure of the lipid interdigitation shows the similar tendency as R_{Li} under stretching simulations (see Fig. A2.2). Therefore, R_{Li} was used as an evaluation index for the transition to the interdigitated gel-like phase.

The first step in the pore formation process is the creation of a chain of water molecules penetrating the bilayer [31,100]. The areal strain, where the water chain is formed, was defined as the critical areal strain ε_c in the US simulations. Because the applied areal strains were discretized in the QS simulations, not only the minimum value of areal strain with a pore, but also the maximum value without a pore in the QS simulation, were analyzed. The actual ε_c in the QS simulation was expected to be within this range.

Data obtained in unsteady MD simulations, e.g., the critical areal strain, are quite-limited because of the limitation of currently available computational power. To obtain quantitative implications from the limited data, standard statistical analyses were used. The critical areal strains obtained in the US simulations were influenced by two factors: the system composition and the stretching speed. To test these effects, a two-way analysis of variance (ANOVA) on the critical areal strain was performed. When the interaction effect was significant, the tests of the simple main effect and multiple comparison (Ryan's method) were performed as post-hoc procedures. The differences were considered to be statistically significant at $p < 0.05$.

4.3. RESULTS

4.3.1. Pore Formation Process

Representative snapshots of the stretched DPPC/cholesterol bilayers in the US and QS simulations are shown in Fig 4.1. In all stretching simulations, the thickness of the bilayer decreases with stretching (Fig. 4.1 *a*–*c*) and, when ε_A exceeds a certain value, which corresponds to ε_c, water molecules penetrate into the central part of the bilayer (Fig. 4.1 *d*). The number of water molecules inside the bilayer quickly increases and a water-filled pore penetrating the bilayer is formed (Fig. 4.1 *e*). From a visual inspection of snapshots of the DPPC/cholesterol bilayers under stretching, three remarkable characteristics of the pore formation process were found. (i) Just before pore formation, the molecular orientations, e.g., the orientation direction of cholesterol molecules or the configurations of DPPC tails, are more ordered in lower-speed stretching simulations (Fig. 4.1 *c*, *f*, and *g*). (ii) The pore formation patterns vary depending on the stretching speed. Two patterns of pore formation in the simulation box were observed in the US simulations; single pore and pores (multi-pore) formations (Fig. 4.1 *h* and *i*). In the multi-pore formation, small pores are temporarily formed in small area [32]. The probabilities, where multi-pore formation was observed, are summarized in Table 4.1. The probability increases with an increase in the stretching speed. (iii) The pore edges of the DPPC/cholesterol bilayer in the US simulations with $c = 0.025$ and 0.05 m/s and the QS simulations are not fully lined with the hydrophilic head groups of lipid molecules, i.e., hydrophobic pore (Fig. 4.1 *e*), unlike a hydrophilic pore [76], whose edge is not lined in pure phospholipid bilayers. For higher-speed stretching simulation, because the structure of the pore changes rapidly with continuous stretching after pore formation in the system with periodic boundary conditions, the pore edge structure is difficult to examine by visual inspection. In the pure DPPC bilayer, there are several differences from the DPPC/cholesterol bilayer. In particular, the pore structure is a typical hydrophilic pore, the molecular orientations are insensitive to the stretching speed, and multi-pore formation occurs more frequently. The overall tendency in the pore formation process in the pure DPPC bilayer is consistent with the results from the previous US

simulations for pure POPC bilayers [32].

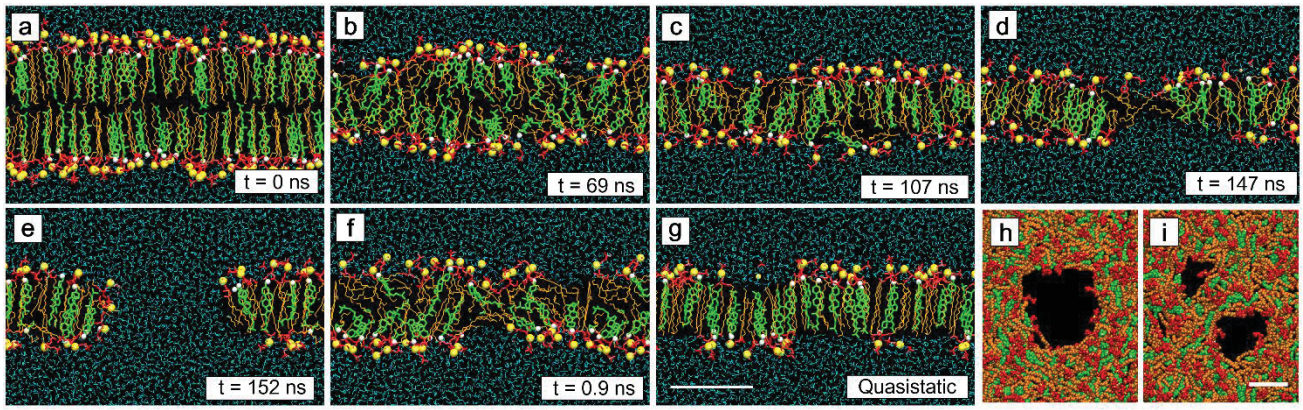

FIGURE 4.1 Representative snapshots of DPPC/cholesterol bilayers before stretching (*a*), under unsteady stretching with c = 0.025 (*b*–*e*) and 3.00 m/s (*f*, *h*, and *i*), and QS simulations (*g*). Panels (*a*–*g*) are side cross-sectional views and (*h*) and (*i*) are top views. The areal strains of the bilayers are 0.00 (*a*), 0.60 (*b*), 1.00 (*c*, *f*, and *g*), 1.44 (*d*), 1.51 (*e*), and 2.40 (*h* and *i*). The DPPC head groups are shown in red, the DPPC tails in orange, the cholesterol molecules in green, the water molecules in blue, the phosphorous atoms in the DPPC molecules as yellow spheres, and the hydrogen atoms in the cholesterol molecules as white spheres. The water molecules in panels (*h*) and (*i*) are not shown, for clarity. The white bars in panels (*g*) and (*i*) correspond to 3 nm.

4.3.2. Molecular Orientation

From a visual inspection of snapshots of the bilayers, the orientations of DPPC and cholesterol molecules just before pore formation depend upon the stretching speed (Fig. 4.1 *c*, *f*, and *g*). As a measure of the molecular orientations of DPPC and cholesterol molecules, the instantaneous order parameter $\hat{S}_{CD}$ and the cholesterol tilt angle θ_c were evaluated. Figure 4.2 shows the relationships between $-\hat{S}_{CD}$ and the areal strain ε_A. In the QS simulation for the DPPC/cholesterol bilayer (Fig. 4.2 *A*), the change in $-\hat{S}_{CD}$ with an increase of ε_A depends strongly on the range of ε_A, as reported previously [77]. $-\hat{S}_{CD}$ decreases in the range $0.00 \le \varepsilon_A \le 0.30$, recovers slightly in the range $0.30 < \varepsilon_A < 0.80$ and relatively sharply in the range $0.80 \le \varepsilon_A < 1.00$, peaks at $\varepsilon_A = 1.00$, and decreases again over the range $1.00 < \varepsilon_A < \varepsilon_c$. In the US simulations with c =0.025 and 0.05 m/s, a similar recovery in $-\hat{S}_{CD}$ occurs after exceeding $\varepsilon_A = 0.80$, although in the US simulations with c ≥ 0.30 m/s, $-\hat{S}_{CD}$

decreases monotonically until pore formation is initiated ($\varepsilon_A < \varepsilon_c$). For the pure DPPC bilayer (Fig. 4.2 *B*), $-\hat{S}_{CD}$ decreases monotonically in all US and QS simulations, and $-\hat{S}_{CD}$ for c = 0.025 and 0.05 m/s is similar to that in the QS simulations.

Figure 4.3 shows relationships between the tilt angle of cholesterol molecules, θ_c, and the areal strain. (The vertical axis in Fig. 4.3 is inverted for easy comparison with Fig. 4.2.) The tendency for θ_c is similar to the inverse for $-\hat{S}_{CD}$. However, θ_c in the QS simulation peaks at ε_A = 0.90, which is slightly smaller than the peak position of $-\hat{S}_{CD}$.

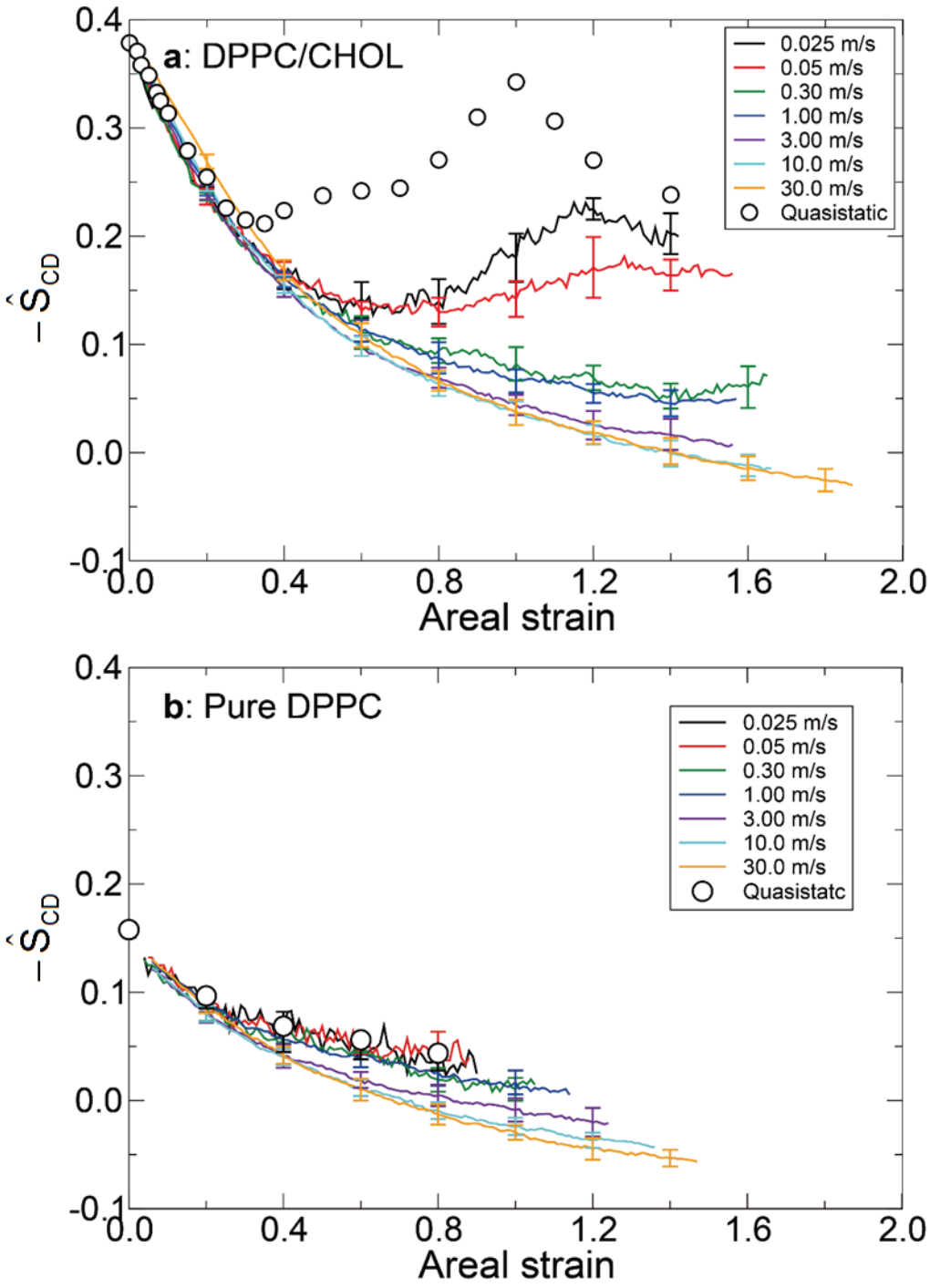

FIGURE 4.2 Lipid chain order parameter $-\widehat{S}_{CD}$ versus areal strain in the DPPC/cholesterol bilayer (*a*) and the pure DPPC bilayer (*b*). The error bars represent standard deviation.

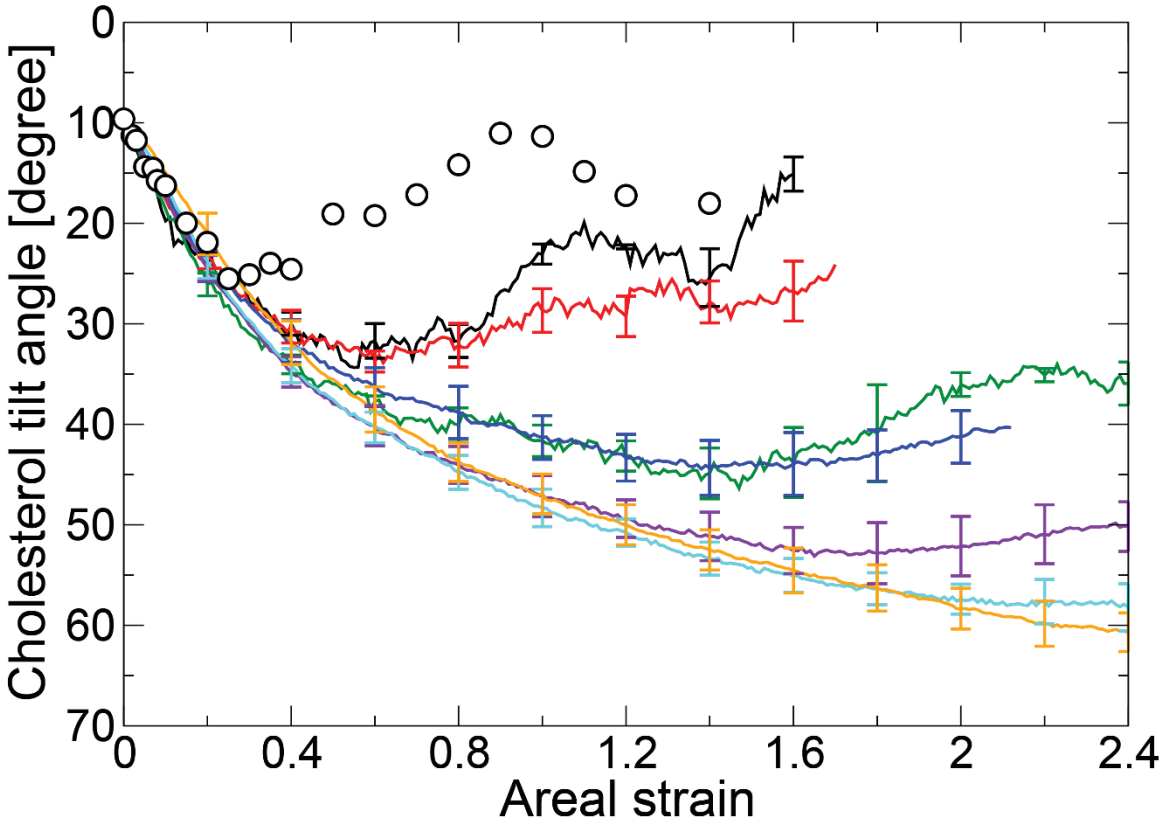

FIGURE 4.3 Cholesterol tilt angle versus areal strain. The vertical axis is inverted for convenient comparison with Fig. 4.2. The error bars represent standard deviation.

4.3.3. Critical Areal Strain

In the QS simulations for the DPPC/cholesterol bilayer, a pore is formed in all triplicate simulations for $\varepsilon_A = 1.40$, whereas no pore is formed in any of the triplicate simulations for $\varepsilon_A = 1.20$. This indicates that the critical areal strain ε_c in the QS simulation is expected to be in the range 1.20 to 1.40. Similar to the DPPC/cholesterol bilayer, ε_c in the QS simulation for the pure DPPC bilayer is expected to be in the range 0.60 to 0.80.

Figure 4.4 shows the relationship between the critical areal strain ε_c and the stretching speed c in the US simulations. The maximum areal strains, where a pore is not formed, and the minimum areal strains, where a pore is formed, obtained in the QS simulations, are also shown in Fig. 4.4 for $c = 0$

m/s. For the pure DPPC bilayer, ε_c increases with increasing stretching speed, with a linear curve in semilogarithmic plots. However, for the DPPC/cholesterol bilayer, ε_c non-monotonically changes with increasing stretching speed and tends to increase slightly. At all stretching speeds, ε_c for the DPPC/cholesterol bilayer is larger than that for the pure DPPC bilayer. The two-way ANOVA test indicates that there is a significant interaction effect between the inclusion of cholesterol and the stretching speed ($p = 0.041$). Tests of simple main effect were performed following the statistical procedure described in the Method section above. The tests show that there are significant effects of cholesterol at all stretching speeds ($p < 0.003$) and significant effects of the stretching speed in both pure DPPC ($p < 10^{-4}$) and DPPC/cholesterol bilayers ($p = 0.001$). Finally, the multiple comparison tests show that ε_c in the pure DPPC bilayer tend to significantly increase with increasing stretching speed. The pairs of ε_c groups in which there is a significant difference are summarized in the Appendix A2.4. In the DPPC/cholesterol bilayer, ε_c at c =30.0 m/s is significantly larger than those at $c = 0.025$, 0.05, 1.0, or 3.0 m/s ($p = 2.3 \times 10^{-4}$, 1.0×10^{-6}, 0.0017, and 2.0×10^{-6}, respectively). These statistical analyses clearly show that the effects of stretching speed depend on the range of the stretching speed in the DPPC/cholesterol bilayer, whereas those in the pure DPPC bilayer are monotonic. Additionally, the inclusion of cholesterol increases ε_c, regardless of the stretching speed in the range used here. The increasing trend in ε_c with increasing stretching speed and the inclusion of cholesterol are in qualitative agreement with previous simulations [32,77] and experimental studies [8,23]. However, it must be noted that the ε_c value obtained here is about two orders of magnitude larger than that obtained from experiments. This discrepancy will be addressed in the Discussion section.

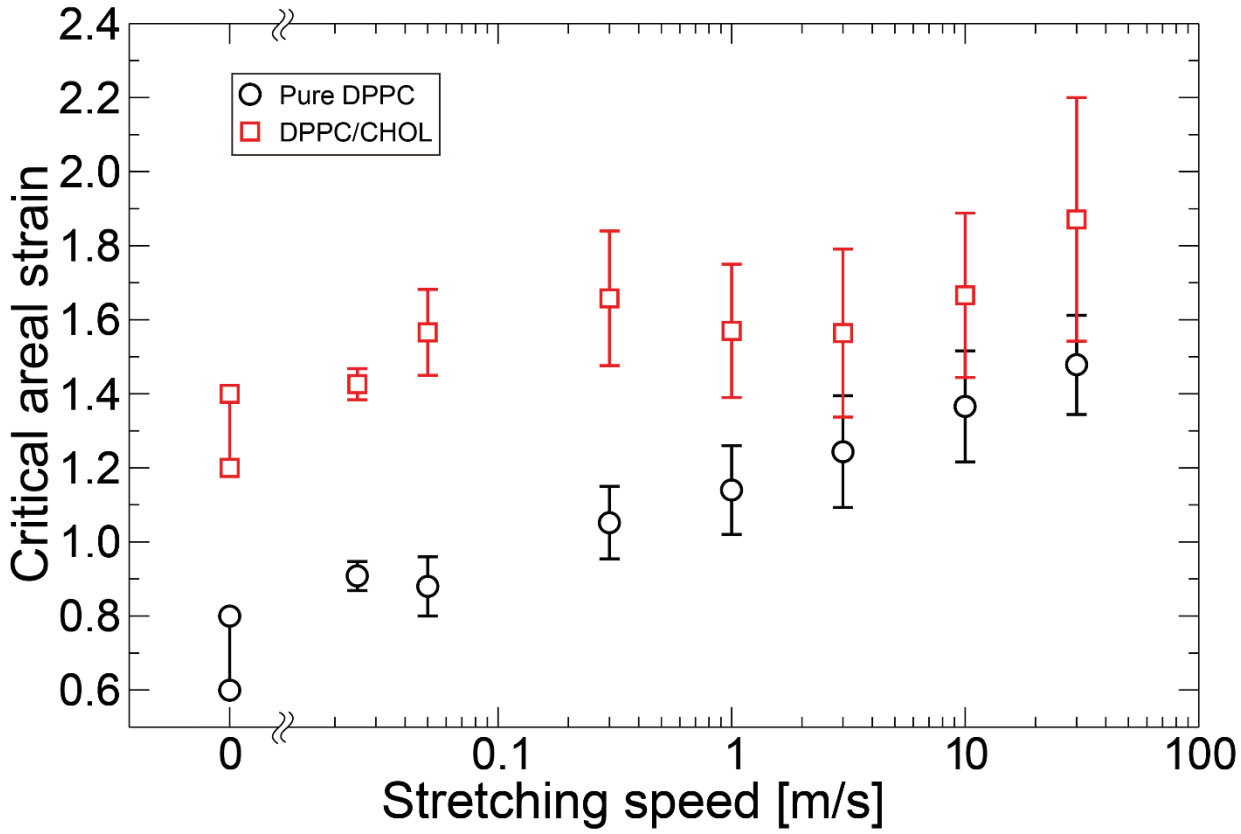

FIGURE 4.4 Critical areal strain ε_c as a function of the stretching speed. Minimum areal strain where the pore forms and maximum areal strain where the pore does not form in the QS simulation are shown here at c = 0.00 m/s. The error bars represent standard deviation.

4.3.4. Bilayer Thickness

The thickness of the bilayer markedly decreases with stretching (Fig. 4.1 *a*–*d*). Figure 4.5 shows the representative relationship between the bilayer thickness and the areal strain. For both the pure DPPC and DPPC/cholesterol bilayers, l_t decreases with increasing ε_A and there is no difference between the simulations at different stretching speeds before pore formation ($\varepsilon_A < \varepsilon_c$). After pore formation ($\varepsilon_A < \varepsilon_c$), l_t for the DPPC/cholesterol bilayer at $c < 3.0$ m/s recovers slightly, but l_t continues to decrease in the other simulations. For the pure DPPC bilayer, the recovery of l_t is observed at $c <$ 10.0 m/s and the recovered amount is larger than that for the DPPC/cholesterol bilayer. Under the same

areal strain, l_t for the DPPC/cholesterol bilayer without a pore is larger than that for the pure DPPC bilayer.

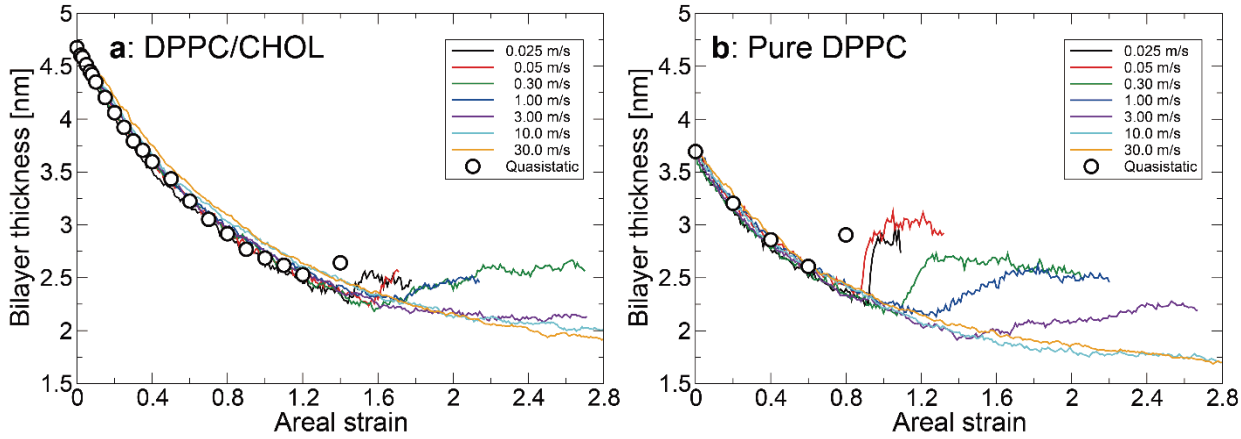

FIGURE 4.5 Representative results of bilayer thickness versus areal strain in the DPPC/cholesterol bilayer (*a*) and the pure DPPC bilayer (*b*).

4.3.5. Stretch-Induced Transition to Interdigitated Gel-like Phase

The relationships between R_{Li} and the stretching speed are shown in Fig. 4.6. With an increase in stretching speed, R_{Li} in the DPPC/cholesterol bilayer decreases under relatively low-speed stretching ($c \leq 0.30$ m/s) and, in contrast, does not markedly change under the relatively high-speed stretching ($c \geq 0.30$ m/s). This trend in R_{Li} occurs because the difference in the order parameter $\hat{S}_{CD}$ between the DPPC/cholesterol and pure DPPC bilayers, where their thicknesses are the same as that for the interdigitated gel-like bilayer, becomes smaller with an increase in stretching speed (inset in Fig. 4.6).

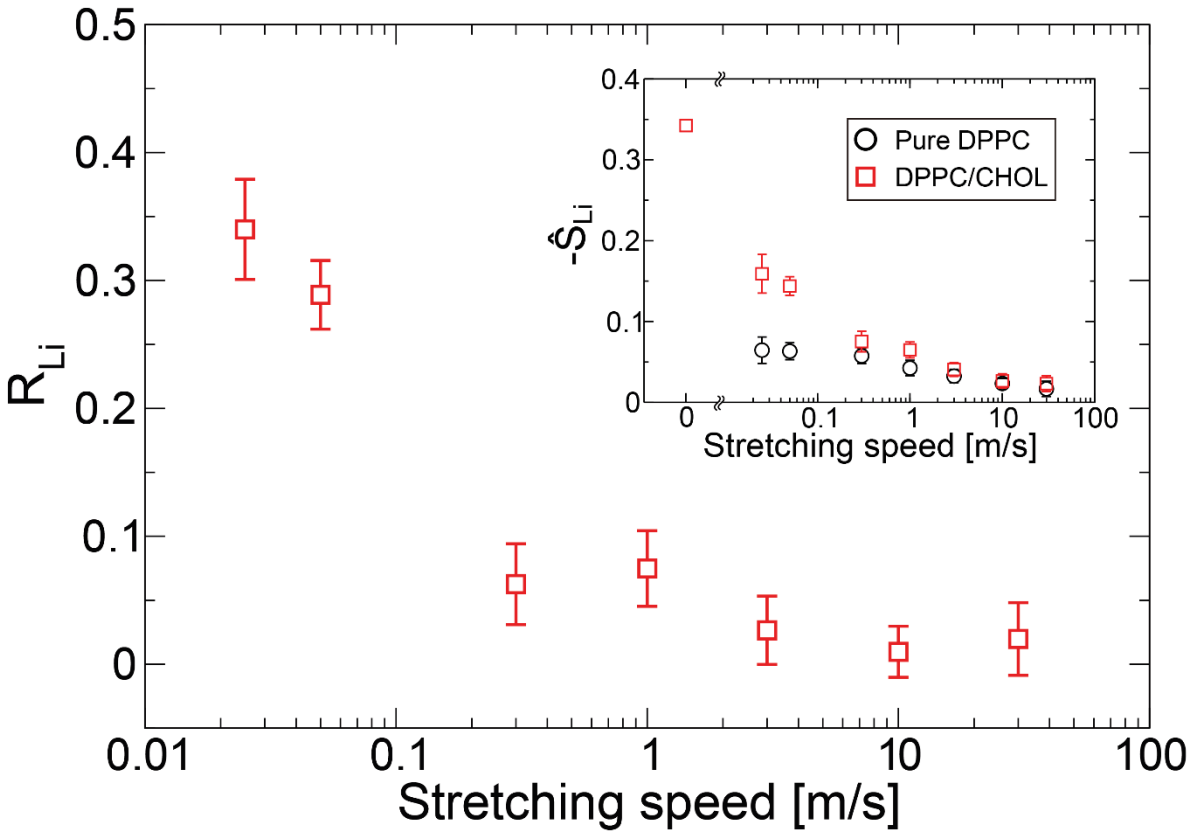

FIGURE 4.6 The relationship between the transition index R_{Li} and the stretching speed. The inset shows the relationship between $-\widehat{S}_{Li}$ and the stretching speed, which is used to calculate R_{Li}. The error bars represent standard deviation.

4.4. DISCUSSION

4.4.1. Interaction Effects of Cholesterol and Stretching Speed

The rupture of the bilayer is a time-dependent phenomenon. Pipette aspiration experiments performed by Evans and coworkers [23] showed that an increase in loading rate induced an increase in rupture tension. They predicted that, at high loading rate, the pore formation during the rupture process became the rate-limiting step, which retards the rupture, resulting in an increase in the rupture tension. Assuming a linear relation between tension and strain, the simulation results here agree qualitatively with the experimental results. A significant increase in critical areal strain in the

simulation here is also confirmed (Fig. 4.4), in spite of the large difference in the range of stretching speed between experiments and simulations. Additionally, the effects of the stretching speed on the critical areal strain in the DPPC/cholesterol bilayer depend upon the range of the stretching speed. The critical areal strain increases at the higher range of stretching speed but does not increase at the lower range. Under lower-speed stretching, the bilayer forms an interdigitated gel-phase-like structure (Fig. 4.1 *c* and *g*), followed by the ordering of DPPC and cholesterol molecules (Figs. 4.2 *a* and 4.3). With an increase in stretching speed, the structural characteristics of the interdigitated gel-like phase becomes ambiguous at the lower range and, in contrast, remain almost constant at the higher range (Fig. 4.6). The results in the Chapter 2 suggested that stretch-induced interdigitation retarded the initiation of the pore formation [77]. Therefore, with an increase in stretching speed at the lower range, pore formation is retarded by its rate-limiting nature and is simultaneously precipitated by the collapse of the interdigitated gel-like bilayer structure, which may be mutually canceled. However, in the higher range, almost no interdigitation occurs and the pore formation is simply retarded by its rate-limiting nature. In summary, the difference in stretching speed effects on the critical areal strain, which depends on the range of the stretching speed, might arise from the dependency on the stretching speed of the stretch-induced ordering with interdigitation.

4.4.2. Discrepancy of Critical Areal Strain between MD Simulation and Experiments

The critical areal strains of planar lipid bilayers obtained in MD simulations range from ~1 to ~2 (Table 4.1). The values are about two orders of magnitude larger than those of RBCs and vesicles obtained in micropipette aspiration experiments (0.01–0.05) [8]. Tolpekina and coworkers [29] showed that the critical areal strain was inversely proportional to the cube root of the reference bilayer area from the free energy model of the bilayer with a pore, considering the finite area in MD simulations. The typical area of the RBCs [101] and the bilayer vesicle [8,23] in experiments ranges from ~100 to

1000 μm^2 and that used here is ~42 nm^2. The range of critical areal strains in the MD simulations here becomes the order of 0.001–0.01 by the scaling, which is close to the range in the experiments. However, it should be noted that the model presented by Tolpekina and coworkers does not consider the effects of stretching speeds. It may be required to develop more sophisticated model including the effects of the reference area and the stretching speed [23] on pore formation, although this is beyond the scope of this study.

4.4.3. Pore Formation in Red Blood Cell Membrane

RBCs have a cholesterol-rich membrane, with a cholesterol concentration in the range 40 to 50 mol% [1], and they have been used as a model of biological cells in various biomechanical experiments [88–90,92]. Li and coworkers [89,93] performed impulse-like stretching experiments for RBCs using laser-induced cavitation. They reported that RBCs can withstand higher areal strain (~0.3) than those obtained in micropipette experiments (~0.05). Additionally, leakage of preloaded calcein from RBCs and RBC rupture does not occur immediately after impulsive stretching, but occurs up to tens of seconds after stretching. They suggested that this time lag was caused by the formation of small pores, which are smaller than calcein and are not detectable in optical measurements.

The previous simulation study in our research group showed that multi-pore formation is observed in pure phospholipid bilayers under high-speed stretching [32]. In this study, under higher speed stretching, the same multi-pore formations are observed in cholesterol-containing bilayers, whose molecular composition is essentially closer to that of the RBC membrane than that of the pure bilayer. The results here show that, although the inclusion of cholesterol affects several mechanical properties of phospholipid bilayers, multi-pore formation is not predominantly limited by cholesterol and provides the potential for multi-pore formation in biological cell membranes.

4.5. CONCLUSION

MD simulation of DPPC/cholesterol and pure DPPC bilayers under unsteady stretching at various stretching speeds provides three observations about the critical areal strain, where the pore is formed. These observations are quantitatively confirmed by standard statistical procedures. (i) The effects of stretching speed on the critical areal strain reported in experiments is also observed in the simulation here despite the much higher stretching speed compared with those applied in the experiments. (ii) The effects of stretching speed in the DPPC/cholesterol bilayer depend on the range of stretching speed and may arise from the dependence of stretch-induced interdigitation on stretching speed. (iii) The effects of cholesterol are not eliminated even under conditions of extremely rapid stretching.

CHAPTER 5. CONCLUSION

In this study, in order to understand molecular details of the cholesterol effects on the rupture of phospholipid bilayers under mechanical stresses, a series of MD simulations of the stretched phospholipid bilayers containing cholesterol molecules was performed. As the rupture process is consisted of two stages, the pore formation in the intact bilayer and the subsequent pore expansion, MD simulations were also divided into two stages. In the Chapter 2, MD simulations of the pore formation in the stretched bilayers containing cholesterol at 0, 20, 40, and 60 mol% were performed. Cholesterol effects on how large areal strain the bilayers can withstand, the pore formation process, and the molecular orientational changes with stretching were evaluated. In the Chapter 3, the equilibrating MD simulations of the cholesterol-containing bilayers starting from those with a pre-formed pore were performed. From the mechanical condition for the spontaneous pore closure, the cholesterol effects on the line tension of the pore edge, which is an energetic loss and prevents the spontaneous expansion of the pore, were estimated. In the Chapter 4, to develop understanding the cholesterol effects on the bilayer rupture, the interaction effects of cholesterol and the stretching speed on the pore formation were investigated by MD simulations of the pure phospholipid and cholesterol-containing bilayers under stretching with various stretching speed. In this chapter, the main results of these chapters are briefly summarized and then the conclusion of this study is presented.

In the Chapter 2, to understand the cholesterol effects on the pore formation in the rupture process, MD simulations of pore formation in stretched DPPC bilayers containing different concentrations of cholesterol (0, 20, 40, and 60 mol%) were performed. With increasing cholesterol concentration, the critical areal strain, where a pore is formed, initially increased, peaked at 40 mol%, and then decreased, which qualitatively agrees with the available experimental data. For the bilayers containing cholesterol, DPPC molecules became disordered at low areal strains, whereas the order slightly increased when the areal strain exceeded a certain value depending on the cholesterol concentration. For 40 mol%

cholesterol, the two monolayers in the bilayer interpenetrate under high areal strains, inducing an increase of the order parameters and the peak positions of the radial distribution function compared with their states at low areal strains, indicating the formation of an interdigitated gel-phase-like structure. The transient increasing of the order of the molecular orientations may inhibit water penetration into the bilayer, resulting in increased critical areal strain in the phospholipid/cholesterol bilayers.

In the Chapter 3, to understand the cholesterol effects on the pore expansion in the rupture process, MD simulations of DPPC bilayer with a pore containing cholesterol in different concentrations (0, 20, and 40 mol%). The bilayers with a pore was obtained by using an equibiaxial stretching simulation. The stretched bilayer with a pore was subsequently compressed and the pore spontaneously closed when the applied areal strain of the bilayer was below a certain value. Using the pore closure areal strain and a free energy model of a stretched bilayer with a pore, the upper and lower limits of the line tensions for the bilayers containing cholesterol at 0, 20, and 40 mol% were estimated to be 17.0–48.2, 54.5–100, and 170–261 pN, respectively. The increasing tendency of the line tension qualitatively agreed with that observed experimentally. The pores in the cholesterol-containing bilayers were lined with several cholesterol molecules, which might increase the bending rigidity of the pore edge, and resulted in the higher line tension of the cholesterol-containing bilayer. The higher line tension promotes the closure of the pore and prevent the expansion in cholesterol-containing bilayers. The considerable dependency of the line tension on the bilayer compositions might be useful to explain the large variations of the transduction efficiency observed with sonoporation treatment.

In the Chapter 4, the effects of stretching speed on mechanical rupture of DPPC/cholesterol bilayers were investigated using unsteady molecular dynamics simulations. The unsteady stretching was modeled by proportional and temporal scaling of atom positions at stretching speeds from 0.025 to 30 m/s. The effects of the stretching speed on the critical areal strain was composed of two regimes. At low speeds (< 1.0 m/s), the critical areal strain was insensitive to speed, whereas it significantly

increaseed at higher speeds. Also, the strain was larger than that of a pure bilayer, regardless of the stretching speeds, which qualitatively agreed with available experimental data. Transient recovery of the cholesterol and phospholipid molecular orientations was evident at lower speeds, suggesting the formation of a stretch-induced interdigitated gel-like phase. However, this recovery was not confirmed at higher speeds or for the pure bilayer. The different responses of the molecular orientations may help explain the two regimes for the effect of stretching speed on pore formation.

MD simulations of cholesterol-containing bilayers here successfully produced the basics cholesterol effects on the structural and mechanical properties of the bilayers (area per lipid, bilayer thickness, lipid tail orientations, cholesterol tilt angle, and area compressibility modulus) at equilibrium as with many previous simulation studies. Additionally, in this study, changes of the critical areal strain, where the pore is formed in MD simulation, with increasing the cholesterol concentration or the stretching speed qualitatively agreed with those where the bilayer rupture occurs in experiments, respectively. Thus, the stretching MD simulations here successfully reproduced the microscopic responses of cholesterol-containing bilayers to mechanical stresses observed experimentally.

The main aim of this study is to understand the molecular-level mechanism of the well-known effects of cholesterol on the mechanical rupture, “Inclusion of cholesterol helps to maintain the membrane integrity under mechanical stresses”, reported by many researchers. According to the molecular-level findings in the MD simulations, the mechanism was deduced as follows. Schematic picture of the rupture of the cholesterol-containing bilayer is shown in Fig. 5.1. When the cholesterol-containing bilayer is exposed to mechanical stretching, phospholipid and cholesterol molecules form the interdigitated gel-like phase structure, in which the membrane molecules interpenetrate and become ordered (Fig. 5.1 g’). Due to the phase transition, the cholesterol-containing bilayer can keep its ordered, in other word, well-packed or condensed structure. Such the bilayer structure is expected to be less permeable to water. As the pore formation is triggered by the water permeation into the

hydrophobic inside of the bilayer, the pore formation is considered to hardly occur in less permeable bilayers. Thus, the inclusion of cholesterol prevent the pore formation in the bilayer. Furthermore, once a pore is formed, the edge of the pore is lined with both the phospholipid and cholesterol molecules (Fig. 5.1 i). The condensed and stiffened cholesterol-containing membrane increases the energetic loss around the pore edge, which means the higher line tension of the pore edge. The higher line tension promotes spontaneous pore closure and prevents the pore expansion and subsequent rupture. In conclusion, the inclusion of cholesterol prevents the bilayer rupture from two aspects: the less permeable stretched bilayer structure and the higher line tension of the pore edge. These are the molecular level mechanisms of the well-known cholesterol effects on mechanical rupture of phospholipid bilayers. This finding will be useful to estimate the maximum intensities of mechanical stresses without the pore formation or the rupture of the cholesterol-containing bilayers. This must contribute to the development of various medical and experimental techniques that require delicate control of not only the membrane rupture but also the pore formation in the biological membranes, e.g., electroporation, sonoporation, and ventricular assisted devices.

Additionally, in the findings of this study, the stretch-induced phase transition to the interdigitated gel-like phase in the cholesterol-containing bilayer is one of the most surprising discovery. This study is the first reports that the combination of the mechanical stretching and the inclusion of cholesterol can induce the phase transition to the interdigitated phase. As the interdigitation is accompanied with drastic structural changes of the membrane, impacts of the interdigitation in biological membranes on the biological functions will be profound. Thus, this finding suggested that the phase transition to the interdigitated phase might be one of the key factors in transduction from mechanical stresses to biological signals via, for example, changes of bilayer properties or structures and functions of membrane proteins in living cells. I believe this finding will encourage the further experimental and simulation studies on the phase behavior of lipid bilayer membranes under mechanical stresses.

This study provided molecular details of the cholesterol effects on the bilayer rupture under

mechanical stresses. Such the molecular level information is inaccessible in current experimental techniques and will be fruitful to understand and control the structures and the functions of bilayer membranes under mechanical stresses in the fields of biological chemistry and medical engineering

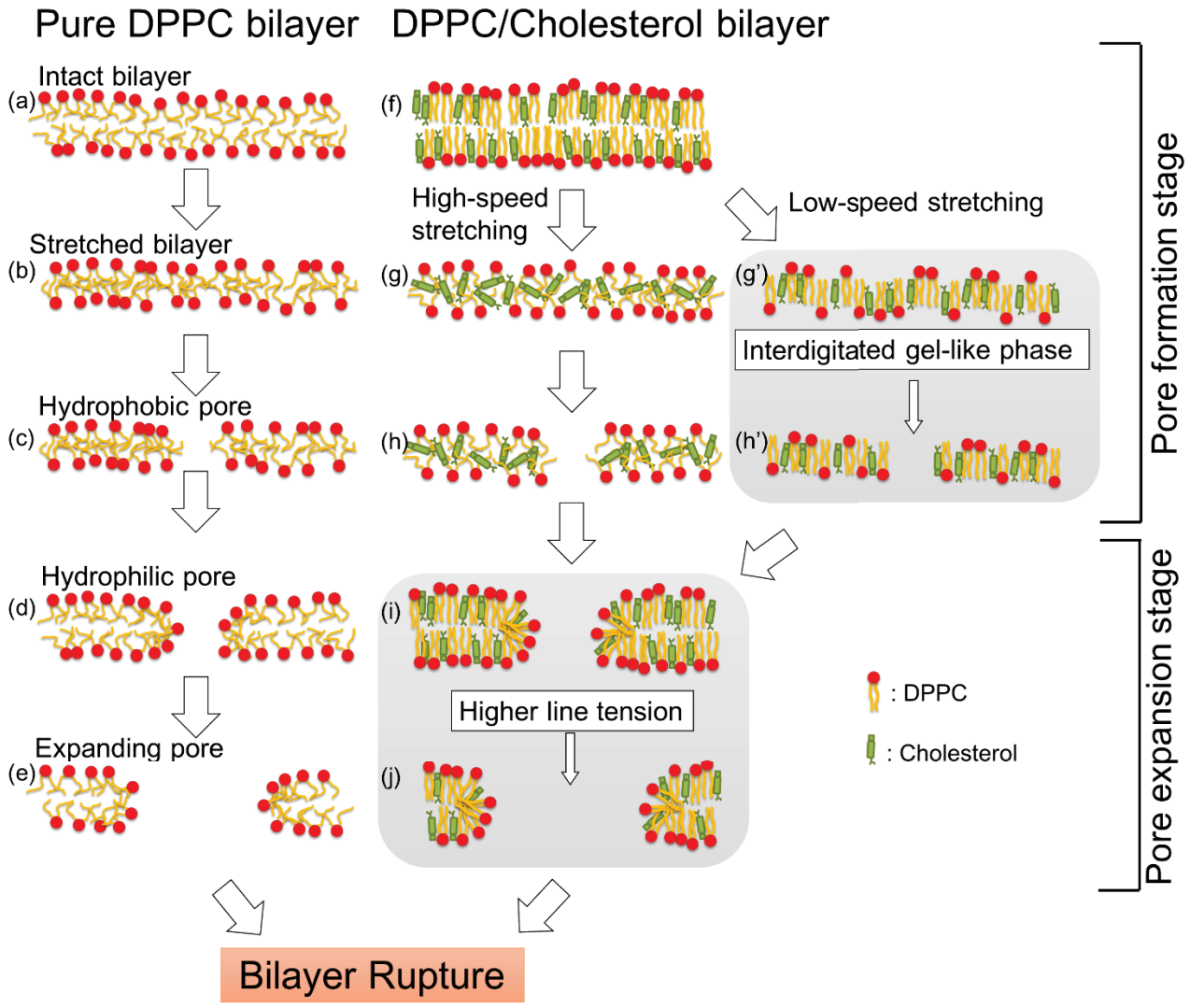

FIGURE 5.1 Schematic picture of the rupture process of cholesterol-containing bilayer.

Appendix 1

Supplementary Information for Chapter 2

A1.1 Initial System

First, two monolayers were constructed by placing DPPC and cholesterol molecules rotated around their long axis on a 10×10 grid (default size: 0.8 nm). These monolayers contained the same number of cholesterol molecules and the position of each molecule was randomly assigned. Then, the two monolayers were stacked to build a bilayer and the entire system was energy minimized. The bilayer was solvated with water molecules, which covered the polar head group of the DPPC and cholesterol molecules. Finally, the solvated system was energy minimized again. To check the effects of the initial molecular positions on the structural properties of the bilayer in the equilibrium state, additional bilayer systems were constructed using the same method with grid size $0.6 - 0.8$ nm and different arrangements of molecules. There was no significant difference in the structural properties after the equilibrium simulation and the construction parameters.

A1.2 Equilibrium Simulation

All MD calculations were carried out under constant temperature (323 K) and pressure (1 bar). The leap-flog algorithm was used for the numerical solution of the equation of motions and the time step was set to 2.0 fs. The PME method [102] with periodic boundary conditions in all directions was used for calculating the Coulombic interactions with a maximum Fourier spacing of 0.12 nm and fitting function in the fourth order. A 1.0-nm cutoff was used for both the van der Waals and short-range Coulombic interactions. The neighbor list was updated every 10 steps and the center of mass motion was removed every step. All bonds were constrained using the linear constraint solver (LINCS) [103] for the DPPC and cholesterol molecules, and the SETTLE algorithm [104] for the water

molecules. The temperatures of DPPC, cholesterol, and water were separately kept constant using the velocity rescaling method [78] with a 0.2 ps coupling constant. The pressure normal and lateral to the bilayer plane were separately maintained using the Parrinello-Rahman method [105] with a 0.5 ps coupling constant.

A1.3 Structural Properties of DPPC/Cholesterol Bilayers

Several typical structural properties of the pure DPPC and DPPC/cholesterol bilayers were calculated and are summarized in Table A1.1. The area per molecule monotonically decreases with increasing cholesterol rate, but there is a relatively small variation between the systems with 40 and 60 mol% compared with the systems of 20 and 40 mol% cholesterol. The area per molecule and its decreasing tendency are in agreement with the previous experimental observations for DMPC/cholesterol bilayers at 303 K [10] and DPPC/cholesterol bilayers at 298 K [39]. The bilayer thickness and average lipid order parameter $-\overline{S}_{CD}$ increase with increasing cholesterol concentration in the range from 0 to 40 mol%, and then slightly decrease between 40 and 60 mol%. The values of the bilayer thickness and $-\overline{S}_{CD}$ in the systems with 0, 20, and 40 mol% cholesterol are in agreement with the experimental measurements for DMPC/cholesterol bilayers at 303 K and DPPC/cholesterol bilayers at 318 K. The A_C value increases with increasing cholesterol concentration, although the difference between 40 and 60 mol% is relatively small. These A_C values mean that the average tilt angles are 18.7, 10.1, and $9.3°$ for S20, S40, and S60, respectively. This decreasing trend of tilt angle is in line with experimental measurements for DPPC/cholesterol membranes at 297 and 333 K [40] and simulation results for DMPC/cholesterol bilayers at 308 K [106]. The differences of all the properties investigated here with increasing cholesterol concentration are small or the general trend reverses from $40-60$ mol% cholesterol, which indicates the phase transition occurs in the range 0 to 40 mol% cholesterol. In fact, according to the phase diagram reproduced by Sankaram and Tompson [41], the pure DPPC bilayer is

a liquid-disordered phase, DPPC bilayers with $10-30$ mol% cholesterol are a combination of liquid-disordered and liquid-ordered systems, and the structure of DPPC bilayers with more than 30 mol% cholesterol is a liquid-ordered phase at this temperature (323 K). This experimental result agrees with the phase transition in the simulations.

TABLE A1.1 Structural parameters of pure DPPC and DPPC/cholesterol bilayers

System label	Cholesterol concentration [mol%]	Area per molecule (system area) [nm^2]	Bilayer thickness* [nm]	Lipid chain order parameter† $-\overline{S}_{CD}$	Cholesterol tilt angle parameter A_C
S00	0	0.65 (65.4)	3.71	0.16	-
S20	20	0.49 (48.7)	4.07	0.28	0.87
S40	40	0.39 (39.2)	4.53	0.38	0.96
S60	60	0.38 (37.6)	4.40	0.36	0.97

*Bilayer thicknesses are represented by the average P–P distance along the bilayer normal.

†Lipid chain order parameters were averaged over *sn*-2 chain.

A1.4 Definition of Cholesterol Tilt Angle

The cholesterol tilt angle θ_C was defined as shown in Fig. A1.1. The carbon atoms of the ring structure connected to the hydroxyl group and the tail are labeled C5 and C21, respectively.

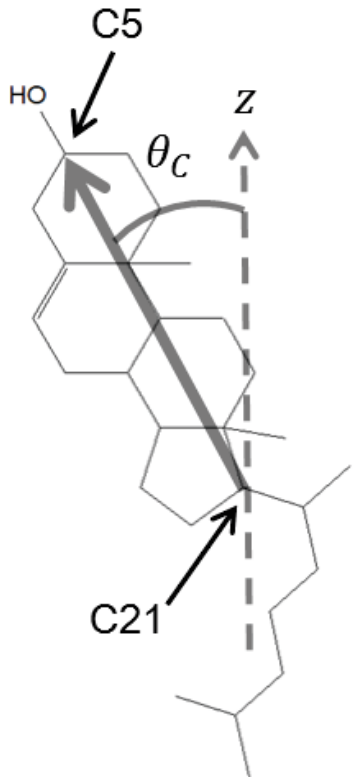

FIGURE A1.1 Definition of the cholesterol tilt angle θ_C and the positions of the C5 and C21 carbon atoms.

A1.5 Comparison between the RDFs

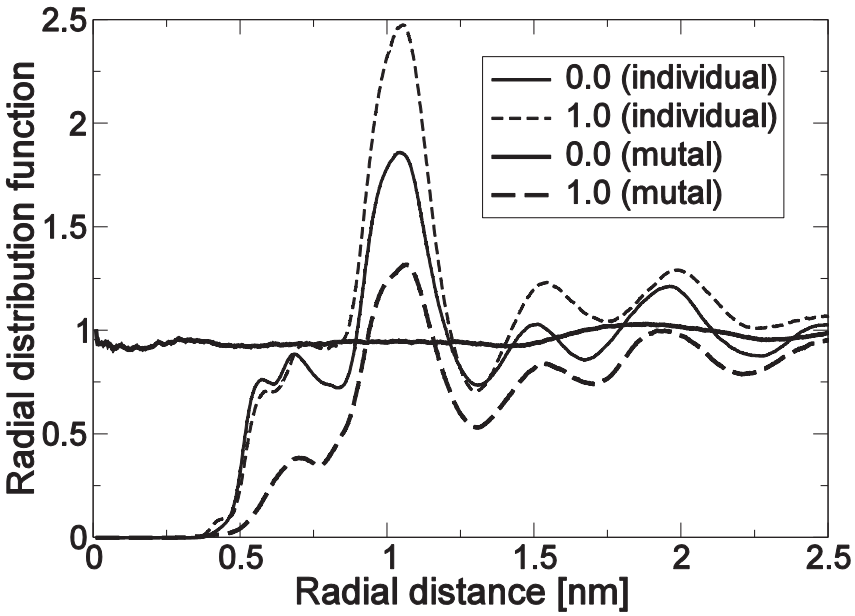

FIGURE A1.2 RDFs of C21 atoms of cholesterol molecules in the stretched bilayers for S40: the RDF calculated from the C21 atoms within the monolayers for $\varepsilon_A = 0.0$ (thin solid line) and 1.0 (thin dashed line), and the RDF calculated for C21 atoms between the upper and lower monolayers for $\varepsilon_A = 0.0$ (thick solid line) and 1.0 (thick dashed line).

A1.6 Verification of Effects of Reference Areas

A previous numerical study [29] has given the maximum areal strain where the pure bilayer maintains its structure without a pore, corresponding to the critical areal strain ε_C, as

$$\varepsilon_C = 3\left\{\frac{\pi}{4}\frac{1}{A_0}\left(\frac{k_C}{K_A}\right)^2\right\}^{\frac{1}{3}}, \tag{A1.1}$$

where A_0, k_C, and K_A are the reference system area, the line tension, and the areal compressibility of the bilayer, respectively. Considering the size of the vesicle in experiments [8] and the area of the bilayer in this study (Table A1.1), the critical areal strains obtained in the simulation were two orders of magnitude smaller, which is roughly in the range of the experimental values. Furthermore, to verify the effects of reference areas on the result shown in Fig. 2.2, Equation A1.1 was applied to the systems here. It is because the current MD simulation was performed at the constant number of lipid and

cholesterol molecules and A_0 decreases with increasing cholesterol concentration (Table A1.1). For appropriate comparison of the critical areal strain under the same reference area, the ratio R, $R = \varepsilon_C(A_0')/\varepsilon_C(A_0) = (A_0/A_0')^{1/3}$, was estimated between the critical areal strains for two systems with the same concentration of cholesterol molecules and the different reference areas A_0 and A_0'. In the case of the system S00 and S40, where the clearest difference of the critical areal strain was obtained, if the system S00 has the same A_0 as system S40 by adjusting *N* for the system S00, the critical areal strain is expected to be 1.18 times larger than that obtained from the original system S00. In the simulations, the critical areal strain (ε_I) for the system S40 is twice as large as that for the system S00. This indicates that differences of the reference system area A_0 do not markedly affect the results here.

Appendix 2

Supplementary Information for Chapter 4

A2.1 Initial System Construction and Equilibration

The procedure for the construction of pure DPPC and DPPC/cholesterol bilayer systems, with almost identical planar bilayer areas and square bilayer shapes, is briefly explained in this section. The fundamental procedure is the same as in the previous study [77]. First, two monolayers were constructed by placing DPPC and cholesterol molecules rotated around their long axis on a 8×8 grid. These monolayers contained the same number of cholesterol molecules and the position of each molecule was assigned randomly. The two monolayers were then stacked up to build a bilayer and the entire system was energy minimized. The bilayer was solvated with water molecules, which immersed the polar head group of DPPC and the cholesterol molecules. The solvated system was energy minimized again and equilibrated by *NPT* MD simulation for more than 100 ns. At this point, the pure DPPC bilayer consisted of 128 DPPC and 4,955 water molecules, and the DPPC/cholesterol bilayer of 76 DPPC, 52 cholesterol, and 4,864 water molecules. Additionally, the bilayer areas of the pure DPPC and DPPC/cholesterol bilayer systems at equilibrium state were 41.87 and 25.12 nm^2, respectively. To reduce the difference in bilayer areas, the DPPC/cholesterol bilayer system was developed further. The square DPPC/cholesterol bilayer system was replicated along the direction parallel to the bilayer plain and a rectangular bilayer system was thus formed. The rectangular bilayer system was deformed using the MD simulation with the deform option, implemented in GROMACS codes, to obtain a square bilayer system. Then, three DPPC and two cholesterol molecules per leaflet were randomly removed from the deformed square bilayer system and the system was equilibrated by *NPT* MD simulation for 10 ns. Once again, eight DPPC and six cholesterol molecules per leaflet were removed and the system was equilibrated for 20 ns. The DPPC/cholesterol bilayer consisted of 128

DPPC and 86 cholesterol molecules. Finally, water molecules were added to both the pure DPPC and DPPC/cholesterol bilayer systems. Both the systems were equilibrated using *NPT* MD simulation for more than 100 ns.

A2.2 Equilibrium Simulation Parameters

Unless otherwise mentioned, all MD calculations were carried out under the conditions shown below. The leap-frog algorithm was used for numerical solution of the equations of motion and the time step was set to 2.0 fs. The PME method [102] with periodic boundary conditions in all directions was used to calculate the Coulombic interactions with 0.12 nm of the maximum Fourier spacing and fitting function in the fourth order. A 1.0-nm cutoff was employed for both van del Waals and short-range Coulombic interactions. The neighbor list was updated every 10 steps and the center of mass motion was removed after every step. All bonds were constrained using the linear constraint solver (LINCS) [103] for the DPPC and cholesterol molecules, and the SETTLE algorithm [104] for the water molecules. The temperatures of DPPC, cholesterol, and water were maintained individually at 323 K using the velocity rescaling method [78] with a 0.2 ps coupling constant. The pressure normal and lateral to the bilayer plane were individually maintained at 1 bar using the Berendsen method [49] with a 0.5-ps coupling constant.

A2.3 Structural Parameters of the Bilayers

To validate the bilayer structures of the pure DPPC and DPPC/cholesterol bilayers before stretching, the typical structural parameters, i.e., area per molecule, bilayer thickness, and the order parameter for the lipid tails, were evaluated. The areas per molecule are 0.656 and 0.391 nm^2 for the pure DPPC and DPPC/cholesterol bilayers, respectively. These are in good agreement with a recent MD simulation study for a DPPC/cholesterol bilayer at 323 K (0.657 and 0.389 nm^2) [54]. However,

the area per molecule for the DPPC/cholesterol bilayer is slightly smaller than those obtained in experiments for similar lipid mixtures [10,39], whereas that for the pure DPPC bilayer is in good agreement with those obtained in experiments (summarized by Nagle and Tristram-Nagle [98]). The bilayer thicknesses are 3.70 and 4.68 nm for the pure DPPC and DPPC/cholesterol bilayers, respectively. As with the area per molecule, the bilayer thicknesses for both bilayers are in good agreement with those obtained in a recent MD simulation study [54] and that for the pure DPPC bilayer is in agreement with experiments for similar lipid bilayers [10]. However, the thickness of the DPPC/cholesterol bilayer is slightly larger than those obtained in experiments with similar lipid mixtures [10]. The averaged order parameter of DPPC tails are 0.16 and 0.38 for the pure DPPC and DPPC/cholesterol bilayers, respectively. These are in good agreement with the recent MD simulation study [54] and in qualitative agreement with experimental measurements [83]. In summary, whereas the structural parameters for the pure DPPC bilayer are in good agreement with those obtained in experiments, those for the DPPC/cholesterol bilayer are slightly different. In particular, the DPPC/cholesterol bilayer in MD simulation tends to be overly condensed, which may be caused by a mismatch in the force field between the DPPC and cholesterol molecules. Meanwhile, the trends in the bilayer structure changes induced by the inclusion of cholesterol are in agreement with both simulations and experimental studies. In conclusion, the bilayer systems used in this study represented real bilayers, without departing from the accuracy of the current MD simulation for lipid mixtures.

A2.4 Detailed Results of Statistical Analyses

In this section, the set of critical areal strains obtained in stretching simulations for a given simulation condition is written as $\varepsilon_c(\phi, c)$. ϕ is a bilayer composition parameter, which is 0 for the pure DPPC bilayer and 1 for the DPPC/cholesterol bilayer, and c is a stretching speed. For example, the set of critical areal strains in the US simulation with c = 0.025 m/s for the DPPC/cholesterol bilayer is

written as $\varepsilon_c(1, 0.025)$. In the results of the statistical procedures, i.e., the two-way ANOVA, the test of the simple main effect, and the multiple comparison test, there are significant differences for the critical areal strain in the pure DPPC bilayer between following pairs: $\varepsilon_c(0, 0.025)$ and $\varepsilon_c(0, c \geq 10.0)$, $\varepsilon_c(0, 0.05)$ and $\varepsilon_c(0, c \geq 3.00)$, $\varepsilon_c(0, 0.30)$ and $\varepsilon_c(0, c \geq 10.0)$, $\varepsilon_c(0, 1.00)$ and $\varepsilon_c(0, 30.0)$, and $\varepsilon_c(0, c \geq 3.00)$ and $\varepsilon_c(0, 30.0)$. This implies that the effects of the stretching speed in the range used here on the critical areal strain are monotonic, except for c = 0.025 m/s, and an increase in stretching speed by about two orders of magnitude induces a significant increase in the critical areal strain.

A2.5 Overlap of DPPC Tails between the Upper and Lower Monolayer

In the interdigitated gel-phase-like structure of the DPPC/cholesterol bilayers under lower speed stretching, the DPPC tails penetrate into the opposite monolayer across the mid-plane of the bilayer, resulting in the overlap of the tails between the upper and lower monolayers (Fig. 4.1 *c* and *g*). The overlap length D_{ol} was defined as $D_{ol} = z_{lower} - z_{upper}$, where z_{lower} and z_{upper} are the average z-positions of the terminal methyl groups of the DPPC tails in the lower and upper monolayers, respectively. D_{ol} will be positive when the tails are interdigitated and will be negative when the tails do not. Figure S1 shows relationships between the overlap length D_{ol} and the areal strain. The overlap lengths in both the pure DPPC and DPPC/cholesterol bilayers are about −0.4 nm before stretching and increase with stretching. In the DPPC/cholesterol bilayer, those during the QS simulation and the US simulations with c = 0.025 and 0.05 m/s considerably increase and become positive. Especially, that in the QS simulation is about 1.3 nm at ε_A = 1.00. However, those with c > 0.30 m/s remain negative during the simulations before the pore formation. In the pure DPPC bilayer, those with c > 0.30 m/s remain negative and those with $c \leq 0.30$ m/s slightly exceed 0.

Figure A2.2 shows the relationships between the stretching speed and the overlap length where the

bilayer thickness becomes congruent with that for the DPPC/cholesterol bilayer under ε_A = 1.00. The overlap length in the DPPC/cholesterol bilayer considerably decreases under relatively low-speed stretching ($c \leq 0.30$ m/s), becomes negative, and slightly decreases under relatively high-speed stretching ($c > 0.30$ m/s). This trend in the overlap length in the DPPC/cholesterol bilayer is very similar to the trend in R_{Li} (Fig. 4.6). In the pure DPPC bilayer, the overlap length in the all stretching simulations remains negative.

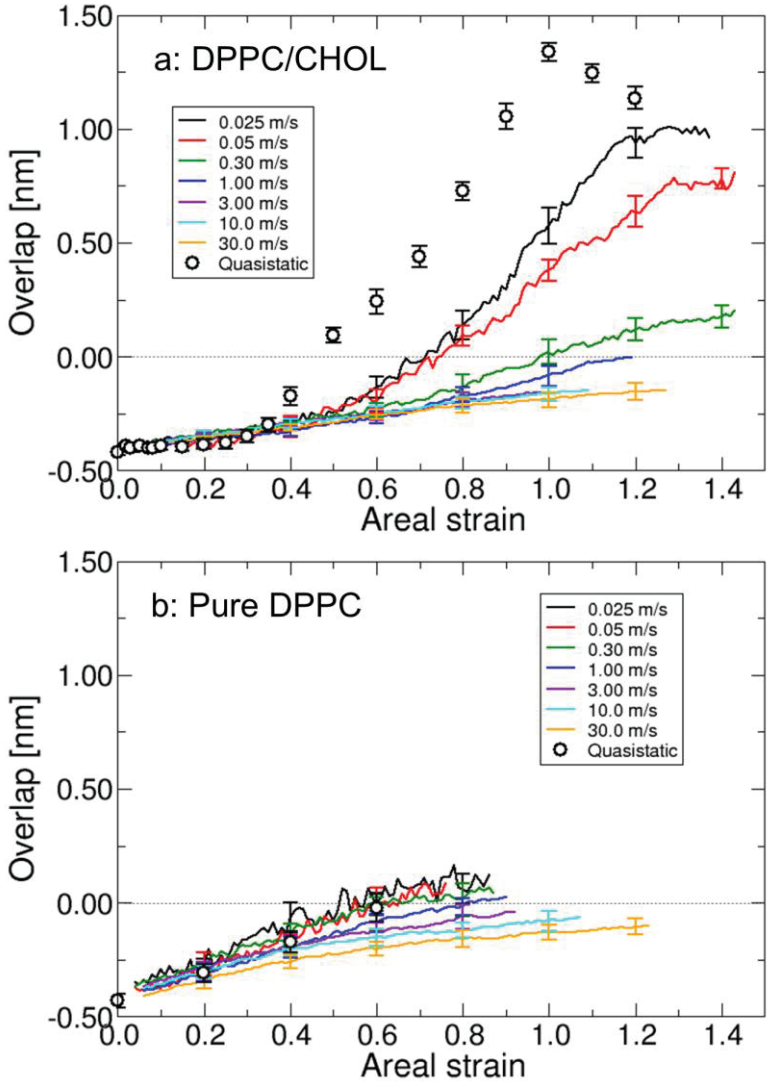

FIGURE A2.1 The relationship between the overlap length and the areal strain ε_A in the DPPC/cholesterol bilayer (a) and the pure DPPC bilayer (b). The overlap length will be positive when the DPPC tails are interdigitated and will be negative when the tails are not. The error bars represent standard deviation.

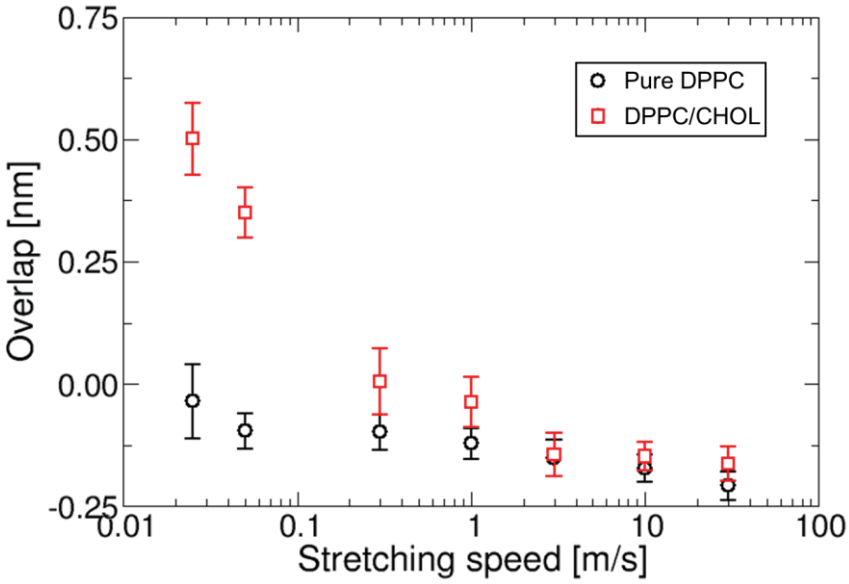

FIGURE A2.2 The relationships between the stretching speed and the overlap length where the bilayer thickness becomes congruent with that for the DPPC/cholesterol bilayer under ε_A = 1.00. The error bars represent standard deviation.

REFERENCES

[1] Alberts, B., Bray, D., Lewis, J., Raff, M., Roberts, K., and Watson, J. D., 1994, Molecular biology of the cell, Garland Publishing, New York.

[2] Vance, D., and Bosch, H. Van den, 2000, "Cholesterol in the year 2000," Biochim. Biophys. Acta, **1529**, pp. 1–8.

[3] Yeagle, P. L., 1985, "Cholesterol and the cell membrane," Biochim. Biophys. Acta, **822**, pp. 267–287.

[4] Mouritsen, O. G., and Zuckermann, M. J., 2004, "What's so special about cholesterol?," Lipids, **39**(11), pp. 1101–1113.

[5] Demel, R., 1972, "The effect of sterol structure on the permeability of lipomes to glucose, glycerol and Rb+," Biochim. Biophys. Acta, **255**, pp. 321–330.

[6] Almeida, P. F., Vaz, W. L., and Thompson, T. E., 1992, "Lateral diffusion in the liquid phases of dimyristoylphosphatidylcholine/cholesterol lipid bilayers: a free volume analysis.," Biochemistry, **31**(29), pp. 6739–6747.

[7] Pike, L. J., 2009, "The challenge of lipid rafts.," J. Lipid Res., **April Supp**, pp. S323–S328.

[8] Needham, D., and Nunn, R. S., 1990, "Elastic deformation and failure of lipid bilayer

membranes containing cholesterol.," Biophys. J., **58**(4), pp. 997–1009.

[9] Róg, T., Pasenkiewicz-Gierula, M., Vattulainen, I., and Karttunen, M., 2009, "Ordering effects of cholesterol and its analogues.," Biochim. Biophys. Acta, **1788**(1), pp. 97–121.

[10] Hung, W. C., Lee, M. T., Chen, F. Y., and Huang, H. W., 2007, "The condensing effect of cholesterol in lipid bilayers.," Biophys. J., **92**(11), pp. 3960–3967.

[11] Ohvo-Rekilä, H., Ramstedt, B., Leppimäki, P., and Slotte, J. P., 2002, "Cholesterol interactions with phospholipids in membranes.," Prog. Lipid Res., **41**(1), pp. 66–97.

[12] Berkowitz, M. L., 2009, "Detailed molecular dynamics simulations of model biological membranes containing cholesterol.," Biochim. Biophys. Acta, **1788**(1), pp. 86–96.

[13] Niemelä, P. S., Hyvönen, M. T., and Vattulainen, I., 2009, "Atom-scale molecular interactions in lipid raft mixtures.," Biochim. Biophys. Acta, **1788**(1), pp. 122–135.

[14] Róg, T., and Vattulainen, I., 2014, "Cholesterol, sphingolipids, and glycolipids: What do we know about their role in raft-like membranes?," Chem. Phys. Lipids, **184**, pp. 82–104.

[15] Koronkiewicz, S., and Kalinowski, S., 2004, "Influence of cholesterol on electroporation of bilayer lipid membranes: chronopotentiometric studies.," Biochim. Biophys. Acta, **1661**(2), pp. 196–203.

[16] Gehl, J., 2003, "Electroporation: theory and methods, perspectives for drug delivery, gene

therapy and research.," Acta Physiol. Scand., **177**(4), pp. 437–447.

[17] Delalande, A., Kotopoulis, S., Postema, M., Midoux, P., and Pichon, C., 2013, "Sonoporation: mechanistic insights and ongoing challenges for gene transfer.," Gene, **525**(2), pp. 191–199.

[18] Rother, R., Bell, L., Hillmen, P., and Gladwin, M. T., 2005, "The clinical sequelae of intravascular hemolysis and extracellular plasma hemoglobin," J. Am. Med. Assoc., **293**(13), pp. 1653–1662.

[19] Harvey, R. D., Ara, N., Heenan, R. K., Barlow, D. J., Quinn, P. J., and Lawrence, M. J., 2013, "Stabilization of distearoylphosphatidylcholine lamellar phases in propylene glycol using cholesterol.," Mol. Pharm., **10**(12), pp. 4408–17.

[20] Schroeder, A., Kost, J., and Barenholz, Y., 2009, "Ultrasound, liposomes, and drug delivery: principles for using ultrasound to control the release of drugs from liposomes.," Chem. Phys. Lipids, **162**(1-2), pp. 1–16.

[21] Lee, S., Kim, D., and Needham, D., 2001, "Equilibrium and dynamic interfacial tension measurements at microscopic interfaces using a micropipet technique. 2. Dynamics of phospholipid monolayer formation," Langmuir, **17**, pp. 5544–5550.

[22] Rawicz, W., Smith, B. A., McIntosh, T. J., Simon, S. A., and Evans, E., 2008, "Elasticity, strength, and water permeability of bilayers that contain raft microdomain-forming lipids," Biophys. J., **94**(12), pp. 4725–4736.

[23] Evans, E., Heinrich, V., Ludwig, F., and Rawicz, W., 2003, "Dynamic tension spectroscopy and strength of biomembranes.," Biophys. J., **85**(4), pp. 2342–2350.

[24] Helfrich, W., 1973, "Elastic properties of lipid bilayers: theory and possible experiments.," Z. Naturforsch. C., **28**(11), pp. 693–703.

[25] Litster, J. D., 1975, "Stability of lipid bilayers and red blood cell membranes," Phys. Lett. A, **53**(3), pp. 193–194.

[26] Helfrich, W., 1974, "The size of bilayer vesicles generated by sonication," Phys. Lett. A, **50**(2), pp. 115–116.

[27] Glaser, R., and Leikin, S., 1988, "Reversible electrical breakdown of lipid bilayers: formation and evolution of pores," Biochim. Biophys. Acta, **940**, pp. 275–287.

[28] Hamada, T., Hirabayashi, Y., Ohta, T., and Takagi, M., 2009, "Rhythmic pore dynamics in a shrinking lipid vesicle," Phys. Rev. E - Stat. Nonlinear, Soft Matter Phys., **80**(5), pp. 1–7.

[29] Tolpekina, T. V, den Otter, W. K., and Briels, W. J., 2004, "Simulations of stable pores in membranes: system size dependence and line tension.," J. Chem. Phys., **121**(16), pp. 8014–8020.

[30] Tieleman, D. P., Marrink, S. J., and Berendsen, H. J., 1997, "A computer perspective of membranes: molecular dynamics studies of lipid bilayer systems.," Biochim. Biophys. Acta, **1331**(3), pp. 235–270.

[31] Tieleman, D. P., Leontiadou, H., Mark, A. E., and Marrink, S. J., 2003, "Simulation of pore formation in lipid bilayers by mechanical stress and electric fields.," J. Am. Chem. Soc., **125**(21), pp. 6382–6383.

[32] Koshiyama, K., and Wada, S., 2011, "Molecular dynamics simulations of pore formation dynamics during the rupture process of a phospholipid bilayer caused by high-speed equibiaxial stretching.," J. Biomech., **44**(11), pp. 2053–2058.

[33] Delemotte, L., and Tarek, M., 2012, "Molecular dynamics simulations of lipid membrane electroporation," J. Membr. Biol., **245**(9), pp. 531–543.

[34] Xie, J. Y., Ding, G. H., and Karttunen, M., 2013, "Molecular dynamics simulations of lipid membranes with lateral force: Rupture and dynamic properties.," Biochim. Biophys. Acta, **1838**(3), pp. 994–1002.

[35] Evans, E., and Needham, D., 1987, "Physical properties of surfactant bilayer membranes: thermal transitions, elasticity, rigidity, cohesion and colloidal interactions," J. Phys. Chem., **91**(16), pp. 4219–4228.

[36] Berger, O., Edholm, O., and Jähnig, F., 1997, "Molecular dynamics simulations of a fluid bilayer of dipalmitoylphosphatidylcholine at full hydration, constant pressure, and constant temperature.," Biophys. J., **72**(5), pp. 2002–2013.

[37] Höltje, M., Förster, T., Brandt, B., Engels, T., von Rybinski, W., and Höltje, H. D., 2001,

"Molecular dynamics simulations of stratum corneum lipid models: fatty acids and cholesterol.," Biochim. Biophys. Acta, **1511**(1), pp. 156–167.

[38] Berendsen, H. J. C., Postma, J. P. M., Gunsteren, W. F. van, and Hermans, J., 1981, "Interaction models for water in relation to protein hydration," Intermolecular Forces, B. Pullman, ed., Reidel, Dordrecht, The Netherlands, p. 331.

[39] McConnell, H., and Radhakrishnan, A., 2003, "Condensed complexes of cholesterol and phospholipids," Biochim. Biophys. Acta, **1610**(2), pp. 159–173.

[40] Murari, R., Murari, M. P., and Baumann, W. J., 1986, "Sterol orientations in phosphatidylcholine liposomes as determined by deuterium NMR.," Biochemistry, **25**(5), pp. 1062–1067.

[41] Sankaram, M. B., and Thompson, T. E., 1991, "Cholesterol-induced fluid-phase immiscibility in membranes.," Proc. Natl. Acad. Sci. U. S. A., **88**(19), pp. 8686–8690.

[42] Chiu, S. W., Jakobsson, E., Mashl, R. J., and Scott, H. L., 2002, "Cholesterol-induced modifications in lipid bilayers: a simulation study.," Biophys. J., **83**(4), pp. 1842–1853.

[43] Hofsäß, C., Lindahl, E., and Edholm, O., 2003, "Molecular dynamics simulations of phospholipid bilayers with cholesterol.," Biophys. J., **84**(4), pp. 2192–2206.

[44] Falck, E., Patra, M., Karttunen, M., Hyvönen, M. T., and Vattulainen, I., 2004, "Lessons of slicing membranes: Interplay of packing, free area, and lateral diffusion in

phospholipid/cholesterol bilayers," Biophys. J., **87**(2), pp. 1076–1091.

[45] Berendsen, H. J. C., van del Spoel, D., and van Drunen, R., 1995, "GROMACS: A message-passing parallel molecular dynamics implementation," Comput. Phys. Commun., **91**, pp. 43–56.

[46] Hess, B., and Kutzner, C., 2008, "GROMACS 4: Algorithms for highly efficient, load-balanced, and scalable molecular simulation," J. Chem. Theory Comput., **4**, pp. 435–447.

[47] Humphrey, W., Dalke, A., and Schulten, K., 1996, "VMD: Visual molecular dynamics," J. Mol. Graph., **14**, pp. 33–38.

[48] Gauthier, A., and Joós, B., 2007, "Stretching effects on the permeability of water molecules across a lipid bilayer.," J. Chem. Phys., **127**(10), p. 105104.

[49] Berendsen, H. J. C., Postma, J. P. M., van Gunsteren, W. F., DiNola, A., and Haak, J. R., 1984, "Molecular dynamics with coupling to an external bath," J. Chem. Phys., **81**(8), pp. 3684–3690.

[50] Leontiadou, H., Mark, A. E., and Marrink, S. J., 2004, "Molecular dynamics simulations of hydrophilic pores in lipid bilayers.," Biophys. J., **86**(4), pp. 2156–64.

[51] Wohlert, J., den Otter, W. K., Edholm, O., and Briels, W. J., 2006, "Free energy of a trans-membrane pore calculated from atomistic molecular dynamics simulations.," J. Chem. Phys., **124**(15), p. 154905.

[52] Kranenburg, M., Venturoli, M., and Smit, B., 2003, "Molecular simulations of mesoscopic bilayer phases," Phys. Rev. E, **67**(6), p. 060901.

[53] Olbrich, K., Rawicz, W., Needham, D., and Evans, E., 2000, "Water permeability and mechanical strength of polyunsaturated lipid bilayers.," Biophys. J., **79**(1), pp. 321–327.

[54] Saito, H., and Shinoda, W., 2011, "Cholesterol effect on water permeability through DPPC and PSM lipid bilayers: a molecular dynamics study.," J. Phys. Chem. B, **115**(51), pp. 15241–15250.

[55] Li, L. K., So, L., and Spector, A., 1985, "Membrane cholesterol and phospholipid in consecutive concentric sections of human lenses.," J. Lipid Res., **26**(5), pp. 600–609.

[56] Doshi, N., Zahr, A. S., Bhaskar, S., Lahann, J., and Mitragotri, S., 2009, "Red blood cell-mimicking synthetic biomaterial particles.," Proc. Natl. Acad. Sci. U. S. A., **106**(51), pp. 21495–21499.

[57] Smith, E. A., and Dea, P. K., 2013, "Differential scanning calorimetry studies of phospholipid membranes: The interdigitated gel phase," Applications of Calorimetry in a Wide Context - Differential Scanning Calorimetry, Isothermal Titration Calorimetry and Microcalorimetry, A.A. Elkordy, ed., InTech, pp. 407–444.

[58] Rahmani, A., Knight, C., and Morrow, M. R., 2013, "Response to hydrostatic pressure of bicellar dispersions containing an anionic lipid: pressure-induced interdigitation.," Langmuir,

29(44), pp. 13481–90.

[59] McIntosh, T. J., McDaniel, R. V., and Simon, S. A., 1983, "Induction of an interdigitated gel phase in fully hydrated phosphatidylcholine bilayers," Biochim. Biophys. Acta - Biomembr., **731**(1), pp. 109–114.

[60] Laggner, P., Lohner, K., Koynova, R., and Tenchov, B., 1991, "The influence of low amounts of cholesterol on the interdigitated gel phase of hydrated dihexadecylphosphatidylcholine," Chem. Phys. Lipids, **60**(2), pp. 153–161.

[61] Smith, E. a, Wang, W., and Dea, P. K., 2012, "Effects of cholesterol on phospholipid membranes: inhibition of the interdigitated gel phase of F-DPPC and F-DPPC/DPPC.," Chem. Phys. Lipids, **165**(2), pp. 151–9.

[62] Kinoshita, M., and Hynynen, K., 2007, "Key factors that affect sonoporation efficiency in in vitro settings: the importance of standing wave in sonoporation.," Biochem. Biophys. Res. Commun., **359**(4), pp. 860–5.

[63] Kudo, N., Okada, K., and Yamamoto, K., 2009, "Sonoporation by single-shot pulsed ultrasound with microbubbles adjacent to cells," Biophys. J., **96**(12), pp. 4866–4876.

[64] Kodama, T., Tomita, Y., Watanabe, Y., Koshiyama, K., Yano, T., and Fujikawa, S., 2009, "Cavitation bubbles mediated molecular delivery during sonoporation," J. Biomech. Sci. Eng., **4**(1), pp. 124–140.

[65] Zhelev, D. V, and Needham, D., 1993, "Tension-stabilized pores in giant vesicles: determination of pore size and pore line tension.," Biochim. Biophys. Acta, **1147**(1), pp. 89–104.

[66] Karatekin, E., Sandre, O., Guitouni, H., Borghi, N., Puech, P.-H., and Brochard-Wyart, F., 2003, "Cascades of transient pores in giant vesicles: line tension and transport.," Biophys. J., **84**(3), pp. 1734–1749.

[67] Portet, T., and Dimova, R., 2010, "A new method for measuring edge tensions and stability of lipid bilayers: effect of membrane composition," Biophys. J., **99**(10), pp. 3264–3273.

[68] Akimov, S. A., Mukovozov, A. A., Voronina, G. F., Chizmadzhev, Y. A., and Batishchev, O. V., 2014, "Line tension and structure of through pore edge in lipid bilayer," Biochem. Suppl. Ser. A Membr. Cell Biol., **8**(4), pp. 297–303.

[69] West, A., Ma, K., Chung, J. L., and Kindt, J. T., 2013, "Simulation studies of structure and edge tension of lipid bilayer edges: Effects of tail structure and force-field," J. Phys. Chem. A, **117**(32), pp. 7114–7123.

[70] de Joannis, J., Jiang, F. Y., and Kindt, J. T., 2006, "Coarse-grained model simulations of mixed-lipid systems: composition and line tension of a stabilized bilayer edge.," Langmuir, **22**(3), pp. 998–1005.

[71] Wang, H., de Joannis, J., Jiang, Y., Gaulding, J. C., Albrecht, B., Yin, F., Khanna, K., and Kindt, J. T., 2008, "Bilayer edge and curvature effects on partitioning of lipids by tail length:

atomistic simulations.," Biophys. J., **95**(6), pp. 2647–2657.

[72] Gurtovenko, A. a, and Vattulainen, I., 2007, "Molecular mechanism for lipid flip-flops.," J. Phys. Chem. B, **111**(48), pp. 13554–9.

[73] Leontiadou, H., Mark, A. E., and Marrink, S.-J., 2007, "Ion transport across transmembrane pores.," Biophys. J., **92**(12), pp. 4209–15.

[74] Karal, M. A. S., Alam, J. M., Takahashi, T., Levadny, V., and Yamazaki, M., 2015, "Stretch-activated pore of the antimicrobial peptide, magainin 2," Langmuir, **31**(11), pp. 3391–3401.

[75] Leontiadou, H., Mark, A. E., and Marrink, S. J., 2004, "Molecular dynamics simulations of hydrophilic pores in lipid bilayers.," Biophys. J., **86**(4), pp. 2156–2164.

[76] Marrink, S. J., de Vries, A. H., and Tieleman, D. P., 2009, "Lipids on the move: simulations of membrane pores, domains, stalks and curves.," Biochim. Biophys. Acta, **1788**(1), pp. 149–168.

[77] Shigematsu, T., Koshiyama, K., and Wada, S., 2014, "Molecular dynamics simulations of pore formation in stretched phospholipid/cholesterol bilayers.," Chem. Phys. Lipids, **183**, pp. 43–49.

[78] Bussi, G., Donadio, D., and Parrinello, M., 2007, "Canonical sampling through velocity rescaling.," J. Chem. Phys., **126**(1), p. 014101.

[79] Abiror, I. G., Arakelyan, V. B., Chernomordik, L. V., Chizmadzhev, Y. A., Pastushenko, V. F., and Tarasevich, M. R., 1979, "Electric breakdown of bilayer lipid membranes I. The main experimental facts and their qualitative discussion," Bioelectrochemistry Bioenerg., **6**(1), pp. 37–52.

[80] Endress, E., Bayerl, S., Prechtel, K., Maier, C., Merkel, R., and Bayerl, T. M., 2002, "The effect of cholesterol, lanosterol, and ergosterol on lecithin bilayer mechanical properties at molecular and microscopic dimensions: A solid-state NMR and micropipet study," Langmuir, **18**(8), pp. 3293–3299.

[81] Nakamura, T., and Shinoda, W., 2013, "Method of evaluating curvature-dependent elastic parameters for small unilamellar vesicles using molecular dynamics trajectory," J. Chem. Phys., **138**(12), p. 124903.

[82] Genova, J., Bivas, I., and Marinov, R., 2014, "Cholesterol influence on the bending elasticity of lipid membranes," Colloids Surfaces A Physicochem. Eng. Asp., **460**, pp. 79–82.

[83] Mills, T., and Toombes, G., 2008, "Order parameters and areas in fluid-phase oriented lipid membranes using wide angle X-ray scattering," Biophys. J., **95**(July), pp. 669–681.

[84] Petelska, A. D., Naumowicz, M., and Figaszewski, Z. A., 2006, "The interfacial tension of the lipid membrane formed from lipid–cholesterol and lipid–lipid systems," Cell Biochem. Biophys., **44**(2), pp. 205–212.

[85] Pichardo, S., Togtema, M., Jackson, R., Zehbe, I., and Curiel, L., 2013, "Influence of cell line

and cell cycle phase on sonoporation transfection efficiency in cervical carcinoma cells under the same physical conditions," IEEE Trans. Ultrason. Ferroelectr. Freq. Control, **60**(2), pp. 432–435.

[86] Duwe, H., and Sackmann, E., 1990, "Bending elasticity and thermal excitations of lipid bilayer vesicles: modulation by solutes," Physica A, **163**, pp. 410–428.

[87] Hochmuth, R. M., 2000, "Micropipette aspiration of living cells," J. Biomech., **33**, pp. 15–22.

[88] Jay, A. W. L., 1973, "Viscoelastic properties of the human red blood cell membrane. I. Deformation, volume loss, and rupture of red cells in micropipettes.," Biophys. J., **13**(11), pp. 1166–1182.

[89] Li, F., Chan, C. U., and Ohl, C. D., 2013, "Yield strength of human erythrocyte membranes to impulsive stretching.," Biophys. J., **105**(4), pp. 872–879.

[90] Lokhandwalla, M., McAteer, J. A., Williams, J. C., and Sturtevant, B., 2001, "Mechanical haemolysis in shock wave lithotripsy (SWL): II. In vitro cell lysis due to shear.," Phys. Med. Biol., **46**(4), pp. 1245–1264.

[91] Quinto-Su, P. a, Kuss, C., Preiser, P. R., and Ohl, C.-D., 2011, "Red blood cell rheology using single controlled laser-induced cavitation bubbles," Lab Chip, **11**(4), pp. 672–678.

[92] Rand, R., and Burton, A., 1964, "Mechanical properties of the red cell membrane: I. Membrane stiffness and intracellular pressure," Biophys. J., **4**(2), pp. 115–135.

[93] Li, F., Chan, C. U., and Ohl, C. D., 2014, "Rebuttal to a comment by Richard E. Waugh on our article 'Yield strength of human erythrocyte membranes to impulsive stretching,'" Biophys. J., **106**(8), pp. 1832–1833.

[94] Fernández, M. L., Marshall, G., Sagués, F., and Reigada, R., 2010, "Structural and kinetic molecular dynamics study of electroporation in cholesterol-containing bilayers.," J. Phys. Chem. B, **114**(20), pp. 6855–6865.

[95] Koshiyama, K., Yano, T., and Kodama, T., 2010, "Self-organization of a stable pore structure in a phospholipid bilayer," Phys. Rev. Lett., **105**(1), p. 018105.

[96] Huang, C.-H., Hsiao, P.-Y., Tseng, F.-G., Fan, S.-K., Fu, C.-C., and Pan, R.-L., 2011, "Pore-spanning lipid membrane under indentation by a probe tip: a molecular dynamics simulation study.," Langmuir, **27**(19), pp. 11930–11942.

[97] Neder, J., West, B., Nielaba, P., and Schmid, F., 2010, "Coarse-grained simulations of membranes under tension.," J. Chem. Phys., **132**(11), p. 115101.

[98] Nagle, J. F., and Tristram-Nagle, S., 2000, "Structure of lipid bilayers," Biochim. Biophys. Acta - Rev. Biomembr., **1469**(3), pp. 159–195.

[99] Koshiyama, K., Kodama, T., Yano, T., and Fujikawa, S., 2006, "Structural change in lipid bilayers and water penetration induced by shock waves: molecular dynamics simulations.," Biophys. J., **91**(6), pp. 2198–2205.

[100] Bennett, W. F. D., and Tieleman, D. P., 2014, “The importance of membrane defects-lessons from simulations.,” Acc. Chem. Res., **47**(8), pp. 2244–2251.

[101] Fung, Y. C., Tsang, W. C., and Patitucci, P., 1981, “High-resolution data on the geometry of red blood cells.,” Biorheology, **18**(3-6), pp. 369–385.

[102] Essmann, U., Perera, L., Berkowitz, M. L., Darden, T., Lee, H., and Pedersen, L. G., 1995, “A smooth particle mesh Ewald method,” J. Chem. Phys., **103**(19), pp. 8577–8593.

[103] Hess, B., Bekker, H., Berendsen, H. J. C., and Fraaije, J. G. E. M., 1997, “LINCS: A linear constraint solver for molecular simulations,” J. Comput. Chem., **18**(12), pp. 1463–1472.

[104] Miyamoto, S., and Kollman, P. A., 1992, “Settle: An analytical version of the SHAKE and RATTLE algorithm for rigid water models,” J. Comput. Chem., **13**(8), pp. 952–962.

[105] Parrinello, M., and Rahman, A., 1981, “Polymorphic transitions in single crystals: A new molecular dynamics method,” J. Appl. Phys., **52**(12), pp. 7182–7190.

[106] Khelashvili, G., Pabst, G., and Harries, D., 2010, “Cholesterol orientation and tilt modulus in DMPC bilayers,” J. Phys. Chem. B, **114**(22), pp. 7524–7534.

PUBLICATION LIST

Original Papers

(i) Taiki Shigematsu, Kenichiro Koshiyama, Shigeo Wada, "Molecular Dynamics Simulations of Pore Formation in Stretched Phospholipid/Cholesterol Bilayers", Chemistry and Physics of Lipids, 183: 43-49 (2014).

(ii) Taiki Shigematsu, Kenichiro Koshiyama, Shigeo Wada, "Effects of Stretching Speed on Mechanical Rupture of Phospholipid/Cholesterol Bilayers: Molecular Dynamics Simulation", Scientific Reports, 5:15369 (2015), DOI:10.1038/srep15369.

(iii) Taiki Shigematsu, Kenichiro Koshiyama, Shigeo Wada, "Line Tension of the Pore Edge in Phospholipid/Cholesterol Bilayer from Stretch Molecular Dynamics Simulation", Journal of Biomechanical Science and Engineering, 15-00422 (2015), DOI:10.1299/jbse.15-00422.

International Conference

(i) Taiki Shigematsu, Kenichiro Koshiyama, Shigeo Wada, "Cholesterol Effects on Rupture of Stretched Phospholipid Bilayer at the Molecular Level", The 3rd International Workshops on Advances in Computational Mechanics, Tokyo, Japan, October 2015 (Invited).

(ii) Taiki Shigematsu, Kenichiro Koshiyama, Ryotaro Kurumatani, Shigeo Wada, "Molecular Perspective of Water Permeability Changes in Phospholipid/Cholesterol Bilayer under Mechanical Stresses", Eighth Asian-Pacific Conference on Biomechanics, Sapporo, Japan,

September 2015.

(iii) Taiki Shigematsu, Kenichiro Koshiyama, Ryotaro Kurumatani, Shigeo Wada, “Energetics of Water Permeation across Stretched Phospholipid/Cholesterol Bilayer: Molecular Dynamics Simulation”, Summer Biomechanics, Bioengineering and Biotransport Conference, Utah, USA, June 2015.

(iv) Taiki Shigematsu, Kenichiro Koshiyama, Shigeo Wada, “Phase Transition and Formation of Transmembrane Pore in Stretched Phospholipid Bilayer Including Cholesterol: Molecular Dynamics Simulation”, Biophysical Journal, 108: Supplement 1, p80a, Maryland, USA, February 2015.

(v) Taiki Shigematsu, Kenichiro Koshiyama, Shigeo Wada, “Pore Formation Dynamics in Phospholipid/Cholesterol Bilayer under Stretching: System Size Dependence”, 3rd International Conference on Molecular Simulation, pp 118, Hyogo, Japan, November 2013.

(vi) Taiki Shigematsu, Kenichiro Koshiyama, Shigeo Wada, “Effects of Cholesterol on Stability of Phospholipid Bilayer to Irreversible Breakdown under Mechanical Stresses: Molecular Dynamics Simulation”, The 7th Asian Pacific Conference on Biomechanics, in USB, Seoul, Korea, August 2013.

(vii) Taiki Shigematsu, Kenichiro Koshiyama, Shigeo Wada, “Molecular Dynamics Simulations of a DPPC/Cholesterol Bilayer under Equibiaxial Stretching”, Ninth International Conference on Flow Dynamics, pp752-753, Miyagi, Japan, September 2012.

Domestic Conference

(i) 重松大輝, 越山顕一朗, 和田成生, ”コレステロールの含有率と引張速さの違いがリン脂質二重膜の破断に与える相互効果：分子動力学シミュレーション”, 日本機械学会関西支部第 90 期定時総会講演会, pp259-260, 京都, 2015 年 3 月.

(ii) 重松大輝, 越山顕一朗, 和田成生, ”引張下コレステロール含有リン脂質二重膜の水分子透過性に関する分子動力学シミュレーション”, 第 27 回バイオエンジニアリング講演会, pp127-128, 新潟, 2015 年 1 月.

(iii) 重松大輝, 越山顕一朗, 和田成生, ”Hydrophobic Pore Formation in Phospholipid/Cholesterol Bilayers under Mechanical Stretching: Molecular Dynamics Simulation”, 第 52 回生物物理学会年会, 3P213, 北海道, 2014 年 9 月.

(iv) 重松大輝, 越山顕一朗, 和田成生, “引張下のコレステロール含有リン脂質二重膜中での L_{β}I 相形成の分子動力学シミュレーション : 力学的要因による溶血現象の解明に向けて”, 日本機械学会 2014 年度年次大会講演, J0240103, 東京, 2014 年 9 月.

(v) 重松大輝, 越山顕一朗, 和田成生, “分子動力学シミュレーションを用いた細胞膜中での臨界可逆孔径の推定”, 第 26 回バイオエンジニアリング講演会, pp261-262, 宮城, 2014 年 1 月.

(vi) 重松大輝, 越山顕一朗, 和田成生, ”Molecular Mechanism of Inhibitory Effect of Cholesterol on Phospholipid Bilayer Rupture: Molecular Dynamics Simulation”, 第 51 回生物物理学会年会, 3P215, 京都, 2013 年 10 月.

(vii) 重松 大輝, 越山 顕一朗, 和田 成生, ”張力下でのコレステロール含有脂質二重膜に形成される孔構造の分子動力学シミュレーション”, 第 25 回バイオエンジニアリング講演会, pp145-146, 茨城, 2013 年 1 月.

(viii) 重松 大輝, 越山 顕一朗, 和田 成生, “準静的引張下におけるコレステロール含有脂質膜の破断:分子動力学シミュレーション”, 第25回計算力学講演会, 2410, 兵庫, 2012 年 10 月.

(ix) 重松 大輝, 越山 顕一朗, 和田 成生, “力学的要因による溶血現象の解明に向けた赤血球膜破断の分子動力学シミュレーション”, 第 23 回バイオフロンティア講演会, pp85-86, 青森, 2012 年 10 月.

(x) 重松 大輝, 越山 顕一朗, 宮崎 浩, 和田 成生, “引張下のコレステロール含有脂質膜の分子動力学シミュレーション”, 日本機械学会 関西学生会平成 23 年度学生員卒業研究発表講演会, pp2-16, 大阪, 2012 年 3 月.

ACKNOWLEDGEMENTS

This study would never have been possible without continuous supports from a great number of people.

Firstly, I would like to express my gratitude to Professor Shigeo Wada for his perceptive comments and encouragement to my research. I was glad and proud to be a member of his laboratory and have the opportunity to study under his supervision. The whole work was carried out in his laboratory at the Graduate School of Engineering Science, Osaka University.

I would like to thank Assistant Professor Kenichiro Koshiyama for his continuous, fruitful, and kind supports. He taught me all aspects of the "conduct of scientific research", including, for example, the skills for designing researches, scientific writing, effective presentation, creating and maintaining computation environments, and enjoying the research life. His continuous guidance and insightful suggestions are greatly helpful for me and my research. Discussions with him were always interesting, meaningful, and promoting my understanding of the topics. I would like to emphasize that this work would not have been completed without his kind and great supports.

I am pleased to thank the thesis defense committee members, Professor Masao Tanaka, Professor Shigenobu Ogata, and Professor Hiroshi Umakoshi for reading the manuscript of this thesis carefully and giving insightful comments about the design of this work and helpful advises from the point of their specialized fields. Their comments made me to realize the new aspects of my research and greatly encouraged me.

I would also like to thank Professor Hiroshi Miyazaki, at Aino University, and Assistant Professor Satoshi Ii for their advices from the point of their fields, biomaterial and computational science, respectively.

I also thank those who are/were the members of Wada laboratory for giving me enjoyable life in Wada laboratory. Especially, I would like to mention the following names: Luosha Xiao, who gave me

lots of sweets; Tomohiro Otani, who gave a lot of advices on the life of Ph.D student; Takayoshi Nishimura, who taught me how to maintain the Wada-Lab calculator cluster “roughly”; Hideaki Ohta, who taught me the difficulty of experiments; Yasunori Kanemori, who is “Magician of Onomatopoeia”; Gabriel Pramudita Saputra, who is a great engineer and a very skilled chef; Ayaka Mizuno, Hayato Amitani, and Shunsuke Iwata, thanks to their supports in the laboratory life, I could concentrate on my work. I’d like to sincerely say “Thank you!” and “I’m sorry…” to them; Takuya Imamura, who can enjoy his life; Naoya Ando, I want to say sorry to him; Ryotaro Kurumatani, who is one of the most industrious and flippant student I have met; Katuki Kashiyama, I want him to enjoy his life.

This work was supported in part by Japan Society for the Promotion of Science (JSPS) Grants-in-Aid for Scientific Research (24240073, 23686031, and 15K01284), Grants-in-Aid for JSPS Fellows (15J05070), and the MEXT project, “Creating Hybrid Organs of the Future” at Osaka University.

Finally, I wish to express my gratitude to my parents, sisters, and brother for their hearty encouragements and continuous supports.

Taiki Shigematsu

Department of Mechanical Science and Bioengineering

Graduate School of Engineering Science

Osaka University